

1 **Inconsistent strategies to spin up models in CMIP5: implications for**
2 **ocean biogeochemical model performance assessment**

3

4 **Roland Séférian^{1*}, Marion Gehlen², Laurent Bopp², Laure Resplandy^{3,2}, James C.**
5 **Orr², Olivier Marti², John P. Dunne⁴, James R. Christian⁵, Scott C. Doney⁶,**
6 **Tatiana Ilyina⁷, Keith Lindsay⁸, Paul R. Halloran⁹, Christoph Heinze^{10,11},**
7 **Joachim Segschneider¹², Jerry Tjiputra¹¹, Olivier Aumont¹³, Anastasia**
8 **Romanou^{14,15}**

9 ¹ CNRM-GAME, Centre National de Recherches Météorologiques-Groupe d'Etude
10 de l'Atmosphère Météorologique, Météo-France/CNRS, 42 Avenue Gaspard Coriolis,
11 31057 Toulouse, France

12 ² LSCE/IPSL, Laboratoire des Sciences du Climat et de l'Environnement, Orme des
13 Merisiers, CEA/Saclay 91198 Gif-sur-Yvette Cedex, France

14 ³ Scripps Institution of Oceanography, UCSD, La Jolla, CA, USA

15 ⁴ Geophysical Fluid Dynamics Laboratory, NOAA, Princeton, New Jersey, USA

16 ⁵ Fisheries and Oceans Canada and Canadian Centre for Climate Modelling and
17 Analysis, Victoria, B.C., Canada

18 ⁶ Marine Chemistry and Geochemistry Department, Woods Hole Oceanographic
19 Institution, Woods Hole MA, USA

20 ⁷ Max Planck Institute for Meteorology, Bundesstraße 53, 20146 Hamburg, Germany

21 ⁸ Climate and Global Dynamics Division, National Center for Atmospheric Research,
22 Boulder, Colorado

23 ⁹ College of Life and Environmental Sciences, University of Exeter, Exeter, EX4

24 4RJ, UK

25 ¹⁰ Geophysical Institute, University of Bergen and Bjerknes Centre for Climate

26 Research, Bergen, Norway

27 ¹¹ Uni Research Climate, Allegt. 55, 5007 Bergen and Bjerknes Centre for Climate

28 Research, Bergen, Norway

29 ¹² University of Kiel, Kiel, Germany

30 ¹³ Sorbonne Universités (UPMC, Univ Paris 06)-CNRS-IRD-MNHN, LOCEAN-

31 IPSL Laboratory, 4 Place Jussieu, F-75005 Paris, France

32 ¹⁴ Dept. of Applied Math. and Phys., Columbia University, 2880 Broadway, New

33 York, NY 10025, USA

34 ¹⁵ NASA-GISS, NY, USA

35

36

37 *Corresponding author address: Roland Séférian, CNRM-GAME, 42 av. Gaspard

38 Coriolis 31100 Toulouse. E-mail: roland.seferian@meteo.fr

39

40 **Abstract**

41 During the fifth phase of the Coupled Model Intercomparison Project (CMIP5)

42 substantial efforts were made to systematically assess of the skill of Earth system

43 models. One goal was to check how realistically representative marine

44 biogeochemical tracer distributions could be reproduced by models. In routine

45 assessments model historical hindcasts were compared with available modern

46 biogeochemical observations. However, these assessments considered neither how

47 close modeled biogeochemical reservoirs were to equilibrium nor the sensitivity of

48 model performance to initial conditions or to the spin-up protocols. Here, we explore

49 how the large diversity in spin-up protocols used for marine biogeochemistry in
50 CMIP5 Earth system models (ESM) contribute to model-to-model differences in the
51 simulated fields. We take advantage of a 500-year spin-up simulation of IPSL-CM5A-
52 LR to quantify the influence of the spin-up protocol on model ability to reproduce
53 relevant data fields. Amplification of biases in selected biogeochemical fields (O_2 ,
54 NO_3 , Alk-DIC) is assessed as a function of spin-up duration. We demonstrate that a
55 relationship between spin-up duration and assessment metrics emerges from our
56 model results and holds when confronted with a larger ensemble of CMIP5 models.
57 This shows that drift has implications for performance assessment in addition to
58 possibly aliasing estimates of climate change impact. Our study suggests that
59 differences in spin-up protocols could explain a substantial part of model disparities,
60 constituting a source of model-to-model uncertainty. This requires more attention in
61 future model intercomparison exercises in order to provide quantitatively more correct
62 ESM results on marine biogeochemistry and carbon cycle feedbacks.

63

64 **1- Introduction**

65 **1-1 Context**

66 Earth system models (ESM) are recognized as the current state-of-the-art global
67 coupled models used for climate research (e.g., Hajima et al., 2014; IPCC, 2013).
68 They expand the numerical representation of the climate system used during the 4th
69 IPCC assessment report (AR4) that was limited to coupled physical general
70 circulation models, to the inclusion of biogeochemical and biophysical interactions
71 between the physical climate system and the biosphere. The ESMs that contributed to
72 CMIP5 substantially differed from each other in terms of their simulations of physical
73 and biogeochemical components of the Earth System. These differences in design

74 translate into a significant variability between the skill with which the different
75 models reproduce the observed biogeochemistry and carbon cycle, which in turn may
76 impact projected climate change responses (IPCC, 2013).

77

78 In the typical objective evaluation and intercomparison of these models, a suite of
79 standardized statistical metrics (e.g., correlation, root-mean-squared errors) are
80 applied to quantify differences between modeled and observed variables (e.g., Doney
81 et al., 2009; Rose et al., 2009; Stow et al., 2009; Romanou et al., 2014; 2015). With
82 the goal of constraining future projections, statistical metrics are often used for model
83 ranking (e.g., Anav et al., 2013), weighting of model projections (e.g., Steinacher et
84 al., 2010) or selection of the most skillful models across a wider ensemble (e.g., Cox
85 et al., 2013; Massonnet et al., 2012; Wenzel et al., 2014). Most of these approaches
86 can be considered as “blind” given that they are routinely applied without considering
87 models’ specific characteristics and treat models *a priori* as equivalently independent
88 of observations. However, since these models are typically initialized from
89 observations, the spin-up procedure (e.g. the length of time for which the model has
90 been run since initialization, and therefore the degree to which it has approached its
91 own equilibrium) has the potential to exert a significant control over the statistical
92 metrics calculated for each model, using those observations.

93

94 **1-2 Initialization of biogeochemical fields and spin-up protocols in CMIP5**

95 Ocean initialization protocols aim at obtaining stable and equilibrated distributions of
96 model state variables, such as temperature or concentrations of dissolved tracers. Most
97 commonly used initialization protocols consist of initializing both physical and
98 biogeochemical variables from either climatologies (derived from the observed fields

99 or previous model simulations) or spatially constant values before running the model
100 to equilibrium. In theory, equilibrium corresponds to steady-state and, hence,
101 temporal derivatives of tracer fields close to zero. The time needed to equilibrate
102 tracer distributions or, in other words, the integration time needed by the model to
103 converge towards its own attractor (which is different from the true state of the
104 climate system) varies greatly between components of the climate system. It spans
105 from several weeks for the atmosphere (e.g., Phillips et al., 2004) to several centuries
106 for ocean and sea ice components (e.g., Stouffer et al., 2004). The equilibration of
107 ocean biogeochemical tracers across the entire water column amounts to several
108 thousands of years (e.g., Heinze et al., 1999; Wunsch and Heimbach, 2008) and
109 depends on the state of background ocean circulation as well as the turbulent mixing
110 and eddy stirring parameterizations (e.g., Aumont et al., 1998; Bryan, 1984;
111 Gnanadesikan, 2004; Marinov et al., 2008). The equilibration time can be different in
112 coupled model configuration (i.e., ocean-atmosphere general circulation models or
113 ESMs) compared to stand-alone climate components due to leaks in the energy budget
114 (Hobbs et al., 2016). In practice, these simulations, called “spin-ups”, often span in
115 general only several hundred of years, at the end of which a quasi-equilibrium state is
116 assumed for the interior ocean tracers.

117

118 The present degree of complexity and spatial as well as temporal resolution of marine
119 biogeochemical ESM components (as well as other physical and chemical
120 components), however, often precludes a spin-up to reach adequate equilibration of
121 biogeochemical tracers. This is a consequence of the large number of state variables
122 present in most of the current generation of biogeochemical models (e.g., for each
123 tracer a separate advection equation has to be solved via a numerical CPU time

124 demanding algorithm), more complex process descriptions (e.g., including more
125 plankton functional types than before), and spatial as well as temporal resolution. This
126 number of state variables has continuously increased from simple biogeochemical
127 models (e.g., HAMOCC3, Maier-Reimer and Hasselmann (1987)) to marine
128 biodiversity models (e.g., Follows et al., 2007). Current generation biogeochemical
129 models embedded in CMIP5 ESMs contain roughly two to four times more state
130 variables than physical models (e.g., atmosphere, ocean, sea-ice), which makes their
131 equilibration computationally costly and difficult. The initialization of
132 biogeochemical state variables is further complicated by the scarcity of
133 biogeochemical observations as compared to observations of physical variables (e.g.,
134 temperature, salinity). So far, three-dimensional observation-based climatologies exist
135 for macro-nutrients, oxygen, dissolved carbon and alkalinity. For other tracers such as
136 dissolved iron, dissolved organic carbon and biomass of the various plankton
137 functional types data are still sparse in space and time in spite of considerable efforts
138 such as the GEOTRACES program for trace elements, or MAREDAT for biomasses
139 of plankton functional types. The latter set of variables is initialized either with
140 constant values (e.g. global average estimates) or with output from a previous model
141 run. An additional difficulty stems from the use of modern climatologies to initialize
142 the ocean state, implicitly assuming a long-term steady state, which does not
143 necessarily represent the preindustrial state of the ocean. These climatologies
144 incorporate the ongoing anthropogenic perturbation of marine biogeochemical fields,
145 be it the uptake of anthropogenic CO₂ or the excess of nutrients inputs and pollutants
146 (e.g., Doney, 2010). Although methods exist to remove the anthropogenic
147 perturbation from some observed ocean carbon tracer fields, their use is still debated
148 since they lead to non-unique results (e.g., Tanhua et al., 2007; Yool et al., 2010).

149

150 The equilibration of marine biogeochemical tracer distributions is driven not only by
151 the ocean circulation but also by numerous internal biogeochemical processes acting
152 at various time scales. For example, while the transport and degradation of sinking
153 organic matter spans days to perhaps several months, the associated impact on deep
154 water chemistry accumulates over several decades to centuries as zones of differential
155 remineralization are mixed across water masses and follows the ocean circulation
156 (Wunsch and Heimbach, 2008). For models including interactive sediment modules,
157 the sediment equilibration takes even longer ($O(10^4)$ years; e.g., Archer et al. (2009)
158 and Heinze et al. (1999)). As a consequence of the interplay between ocean
159 circulation and biogeochemical processes, biogeochemical models require long spin-
160 up times to equilibrate (e.g., Khatiwala et al., 2005; Wunsch and Heimbach, 2008).
161 Modeling studies of paleo-oceanographic passive tracers such as $\delta^{18}\text{O}$ or $\Delta^{14}\text{C}$
162 (Duplessy et al., 1991), or global ocean passive tracers (Wunsch and Heimbach,
163 2008), as well as more recently available modern global scale data compilations (e.g.,
164 Key et al., 2004; Sarmiento and Gruber, 2006) and GEOTRACES Intermediate Data
165 product 2014 (Version 2) <http://www.bodc.ac.uk/geotraces/data/idp2014/>) provide an
166 estimate of the time required for the ocean biogeochemical reservoir to equilibrate
167 with the climate systems (excluding continental weathering and reaction with marine
168 sediments). For the deep water masses, this time is about 1500 years in the Atlantic
169 Ocean and reaches up to 10000 years in the North Pacific Ocean (Wunsch and
170 Heimbach, 2008).

171

172 In a context of model-to-model intercomparison, this time range contributes to the
173 model uncertainty. Lessons from the previous Ocean Carbon Model Intercomparison

174 Project phase 2 (OCMIP-2) exercise have demonstrated that some models required
175 ~10,000 years to reach a state where the global sea-air carbon flux is about 0.01 Pg C
176 y^{-1} .

177

178 While it is recognized that long time-scale processes influence the length of spin-up to
179 equilibrium, the spin-up duration is usually defined *ad hoc* based on external
180 constraints or internal biogeochemical criteria. The computational cost is commonly
181 invoked as external constraint to shorten and limit the spin-up duration. It is directly
182 related to model complexity (e.g., Tjiputra et al., 2013; Vichi et al., 2011; Yool et al.,
183 2013) and spatial resolution (Ito et al., 2010). The internal biogeochemical criteria
184 applied to derive the duration of the spin-up simulations are generally defined by (i)
185 reaching a steady-state, quasi equilibrium of the long-term global-mean CO₂ fluxes
186 between the ocean and the atmosphere (e.g., Dunne et al., 2013; Ilyina et al., 2013;
187 Lindsay et al., 2014; Romanou et al., 2013; Séférian et al., 2013), (ii) determining the
188 amount of carbon stored in the ocean at preindustrial state (e.g., Dunne et al., 2013;
189 Vichi et al., 2011) or (iii) representing relevant biogeochemical tracer patterns (e.g.,
190 oxygen minimum zone in Ito and Deutsch (2013)).

191

192 Despite its importance, only limited information on spin-up procedures is available
193 through the CMIP5 metadata portal (<http://metaforclimate.eu/trac>). Information on
194 spin-up protocols and model initialization is usually not taken into account in model
195 intercomparison studies (e.g., Andrews et al., 2013; Bopp et al., 2013; Cocco et al.,
196 2013; Frölicher et al., 2014; Gehlen et al., 2014; Keller et al., 2014; Resplandy et al.,
197 2013; 2015; Rodgers et al., 2014; Séférian et al., 2014). This information, if available,
198 can only be found separately in the reference papers of individual models (e.g.,

199 Adachi et al., 2013; Arora et al., 2011; Collins et al., 2011; Dunne et al., 2013; Ilyina
200 et al., 2013; Lindsay et al., 2014; Romanou et al., 2013; Séférian et al., 2013; Séférian
201 et al., 2015; Tjiputra et al., 2013; Vichi et al., 2011; Volodin et al., 2010; Watanabe et
202 al., 2011; Wu et al., 2013). The duration of spin-up simulations of CMIP5 ocean
203 biogeochemical components spans from one hundred years (e.g., CMCC-CESM) to
204 several thousand years (e.g., MPI-ESM-LR, MPI-ESM-MR) (Figure 1 and Table 1).
205 Model initialization and spin-up procedures are equally variable across the model
206 ensemble (Figure 1 and Table 1). Four different sources of initialization and four
207 different procedures of model equilibration emerge from the 24 ESMs reviewed for
208 this study.

209

210 Biogeochemical state variables were mostly initialized from observations, although
211 from various releases of the same World Ocean Atlas global climatology (WOA1994,
212 WOA2001, WOA2006, WOA2010). A small subset of ESMs relied either on a mix
213 between previous model output and observations or solely on model output from a
214 previous simulation for initialization. Similarly, spin-up procedures fall into two
215 categories. The first one may be called “sequential”: it consists in decomposing the
216 spin-up integration into one long offline simulation (~200-10000 years) and one
217 shorter online simulation (~100-1000 years). During the offline simulation, the
218 biogeochemical model is forced by dynamical fields from the climate model or from
219 reanalysis (CanESM2, MRI-ESM, Figure 1 and Table 1). Some modeling groups have
220 adopted a “direct” strategy, which consists in running solely one online or coupled
221 spin-up simulation (e.g., CNRM-ESM1, GFDL-ESM2M, GFDL-ESM2G, GISS-E2-
222 H-CC, GISS-E2-R-CC, NorESM1-ME). Finally, a spin-up “acceleration” procedure is
223 used by CMCC-CESM. This technique consists of enhancing the ocean carbon

224 outgassing to remove anthropogenic carbon from the ocean, a legacy from
225 initialization with modern data (Global Data Analysis Project or GLODAP following
226 Key et al., 2004). None of these spin-up procedures, durations and sources of
227 initialization can be considered as “standard”; each of them is unique and subjectively
228 employed by one modeling group.

229

230 Objective arguments and hypotheses justifying the choice of one method of spin-up
231 rather than the others have been the focus of previous studies (e.g., Dunne et al., 2013;
232 Heinze and Ilyina, 2015; Tjiputra et al., 2013). Similarly, individual modeling groups
233 have discussed the impacts of their particular spin-up procedure on model
234 performance individually (e.g., Dunne et al., 2013; Lindsay et al., 2014; Séférian et
235 al., 2013; Vichi et al., 2011). However, no study has addressed the potential for the
236 large diversity of spin-up procedures found across the CMIP5 ensemble to translate
237 into model-to-model differences in terms of comparative model performance
238 assessments or model evaluations in terms of future projections.

239

240 **1-3 Objectives of this study**

241 This study assesses the role of the spin-up protocol in controlling the ‘final’
242 representation of biogeochemical fields, and subsequent model skill assessment,
243 providing a complementary analysis from the studies of Sen Gupta et al. (2012; 2013).
244 It relies on a 500-year long spin-up simulation from a state-of-the-art Earth system
245 model, IPSL-CM5A-LR to investigate the impacts of spin-up strategy on selected
246 biogeochemical tracers and residual model drift across the various ESMs of the
247 CMIP5 ensemble. We demonstrate that the duration of the spin-up has implications
248 for the determination of robust and meaningful skill-score metrics that should improve

249 future intercomparison studies such as CMIP6 (Meehl et al., 2014).

250

251 Section 2 describes the model, the observations, the model experiments, as well as the
252 methods used for assessing the impacts of spin-up protocols on the representation of
253 biogeochemical fields in IPSL-CM5A-LR, as well as across the ensemble of CMIP5
254 ESMs. Section 3 presents the analysis developed for the assessment of the impact of
255 spin-up duration on the representation of biogeochemical structures. Implications and
256 recommendations are discussed in Sections 4 and 5, respectively.

257

258 **2- Methods**

259 **2-1- Model simulations**

260 This study exploits in particular results from one simulation performed with IPSL-
261 CM5A-LR (Dufresne et al., 2013), considered here to be representative of the likely
262 behavior of other CMIP5 Earth system models. Like other current generation of
263 ESMs, IPSL-CM5A-LR combines the major components of the climate system (Chap
264 9, Table 9.1, (IPCC, 2013). The atmosphere is represented by the atmospheric general
265 circulation model LMDZ (Hourdin et al., 2006) with a horizontal resolution of
266 $3.75^\circ \times 1.87^\circ$ and 39 levels. The land surface is simulated with ORCHIDEE (Krinner et
267 al., 2005). The oceanic component is NEMOv3.2 in its ORCA2 global configuration
268 (Madec, 2008). It has a horizontal resolution of about 2° with enhanced resolution at
269 the equator (0.5°) and 31 vertical levels. NEMOv3.2 includes the sea-ice model LIM2
270 (Fichefet and Maqueda, 1997), and the marine biogeochemistry model PISCES
271 (Aumont and Bopp, 2006). PISCES simulates the biogeochemical cycles of oxygen,
272 carbon and the main nutrients with 24 state variables. The model simulates dissolved
273 inorganic carbon and total alkalinity (carbonate alkalinity + borate + water) and the

274 distributions of macronutrients (nitrate and ammonium, phosphate, and silicate) and
275 the micronutrient iron. PISCES represents two sizes of phytoplankton (i.e.,
276 nanophytoplankton and diatoms) and two zooplankton size-classes: microzooplankton
277 and mesozooplankton. PISCES simulates semi-labile dissolved organic matter, and
278 small and large sinking particles with different sinking speeds (3 m d^{-1} and 50 to 200
279 m d^{-1} , respectively). While fixed elemental stoichiometric C:N:P- ΔO_2 ratios after
280 Takahashi et al. (1985) are imposed for these three compartments the internal
281 concentrations of iron, silica and calcite are simulated prognostically. The carbon
282 system is represented by dissolved inorganic carbon, alkalinity and calcite. Calcite is
283 prognostically simulated following Maier-Reimer (1993) and Moore et al. (2002).
284 Alkalinity in the model system includes the contribution of carbonate, bicarbonate,
285 borate, protons, and hydroxide ions. Oxygen is prognostically simulated. The model
286 distinguishes between oxic and suboxic remineralization pathways, the former relying
287 on oxygen as electron acceptor, the latter on nitrate. For carbon and oxygen pools, air-
288 sea exchange follows the Wanninkhof (1992) formulation.

289 The model's boundary conditions account for nutrient supplies from three different
290 sources: atmospheric dust deposition for iron, phosphorus and silica (Jickells and
291 Spokes, 2001; Moore et al., 2004; Tegen and Fung, 1995), rivers for nutrients,
292 alkalinity and carbon (Ludwig et al., 1996) and sediment mobilization for sedimentary
293 iron (de Baar and de Jong, 2001; Johnson et al., 1999). To ensure conservation of
294 nitrogen in the ocean, annual total nitrogen fixation is adjusted to balance losses from
295 denitrification. For the other macronutrients, alkalinity and organic carbon, the
296 conservation is ensured by tuning the sedimental burial to the total external input from
297 rivers and dust. In PISCES, an adequate treatment of external boundary conditions has
298 been demonstrated to be essential for the accurate simulation of nutrient distributions

299 (Aumont and Bopp, 2006; Aumont et al., 2003). Riverine carbon inputs induce a
300 natural outgassing of carbon of 0.6 Pg C y^{-1} which has been shown to be essential to
301 model the inter-hemispheric gradient of atmospheric CO_2 under preindustrial state
302 (Aumont et al., 2001).

303

304 The core simulation used within this study is a 500-year long coupled preindustrial
305 run. It uses the same atmospheric, land surface and ocean configurations as IPSL-
306 CM5A-LR (Dufresne et al., 2013) for which the marine biogeochemistry has been
307 extensively evaluated (see e.g., S  f  rian et al. (2013) for modern-state evaluation).
308 The only difference between the “standard” preindustrial simulation contributed to
309 CMIP5 and the present one is the initial conditions. While the CMIP5 preindustrial
310 simulation starts from an ocean circulation after several thousand years of online
311 physical adjustment, the present simulation starts from an ocean at rest using the
312 January temperature and salinity fields from the World Ocean Atlas (Levitus and
313 Boyer, 1994). Biogeochemical state variables were initialized from data compilations
314 or climatologies as explained in the following section. Atmospheric CO_2 and other
315 greenhouse gases, as well as natural aerosols, were set to their 1850 preindustrial
316 values. The simulation is extensively described in terms of ocean physics by Mignot
317 et al. (2013). Mignot and coworkers show that the strength of the Atlantic meridional
318 overturning circulation and the Antarctic circumpolar current as well as the upper 300
319 m ocean heat content stabilize after 250 years of simulation.

320

321 Although the spin-up protocol used to conduct this 500-year long simulation is not
322 readily comparable to the one used to produce the initial conditions for the CMIP5
323 preindustrial simulation, its duration is greater than the median length of on-line

324 adjustment computed from the multiple spin-up protocols applied during CMIP5
325 (~395 years, Figure 1 and Table 1). Besides, the methodology of initializing
326 biogeochemical state variables from data fields is not broadly employed by the
327 various modeling groups that have contributed to CMIP5. Despite the above-
328 mentioned methodological shortcuts, we take this 500-year long preindustrial
329 simulation as a representative example of a spin-up protocol given the diversity of
330 approaches used by CMIP5 models.

331

332 **2-2- Observations for initialization and evaluation**

333 Two streams of data sets were used in this study. The first stream combines data from
334 the World Ocean Atlas 1994 (WOA94, Levitus and Boyer (1994) and Levitus et al.,
335 (1993)) for the initialization of 3-dimensional fields of temperature and salinity,
336 dissolved nitrate, silicate, phosphate and oxygen, and data from GLODAP (Key et al.,
337 2004) for preindustrial dissolved inorganic carbon and total alkalinity. This stream of
338 data was chosen purposely in our experimental setup to be slightly different than the
339 second stream of data, World Ocean Atlas 2013 (WOA2013, Levitus et al. (2013)),
340 the evaluation data set.

341

342 A second stream of data was used to compare modeled biogeochemical fields. It
343 includes up-to-date observed climatologies of nitrate and oxygen from the WOA2013.
344 This database is based on samples collected since 1965, and including data more
345 recently collected than that made use of in WOA94. For the concentrations of
346 preindustrial dissolved inorganic carbon and total alkalinity, we still use GLODAP.
347 The second stream of data was selected to be as close as possible to the “standard”
348 evaluation procedure of skill-assessment protocols found in CMIP5 model reference

349 papers (Adachi et al., 2013; Arora et al., 2011; Collins et al., 2011; Dunne et al., 2013;
350 Ilyina et al., 2013; Lindsay et al., 2014; Romanou et al., 2013; Séférian et al., 2013;
351 Séférian et al., 2015; Tjiputra et al., 2013; Vichi et al., 2011; Volodin et al., 2010;
352 Watanabe et al., 2011; Wu et al., 2013). Differences between these two streams of
353 data are minor and are further detailed below.

354

355 **2-3- Approach and statistical analysis**

356 To quantify the impacts of a large diversity of spin-up procedures on the
357 representation of biogeochemical fields in CMIP5, we employ a three-fold approach.

358 (1) The 500-year long spin-up simulation described in Section 2.1 is used to
359 determine the influence of the spin-up procedure on the representation of
360 biogeochemical fields in IPSL-CM5A-LR.

361 (2) In the next step, relationships between biases in modeled fields, model-data
362 mismatches and the duration of the spin-up simulation are identified across the
363 CMIP5 ensemble. For this step, drifts in biogeochemical fields are determined from
364 the first century of the preindustrial simulation (referred to as *piControl*) of each
365 CMIP5 ESM.

366 (3) Finally, the ensemble of industrial-revolution to present-day simulation (referred
367 to as *historical*) from each available CMIP5 ESM are used to estimate the impact of
368 these drifts in biogeochemical fields on the ability of models to replicate modern
369 observations. For a given model, we use the ensemble average of the available
370 ‘historical’ members if several realizations are available.

371 For this purpose, several statistical skill score metrics are computed following Rose et
372 al. (2009) and Stow et al. (2009) from model fields interpolated on a regular 1° grid
373 and to fixed depth levels. The skill score metrics are (1) the global averaged

374 concentrations for overall drift; (2) the error or bias between modeled and observed
375 fields at each grid-cell; (3) spatial correlation between model and observations to
376 assess mismatches between modeled and observed large-scale structures; (4) the root-
377 mean squared error (RMSE) to assess the total cumulative errors between modeled
378 and observed fields. These statistical metrics are computed at different depth levels,
379 but for clarity we focus on surface, 150 m (thermocline) and 2000 m (deep) levels.
380 These statistical metrics were chosen among those described in the literature, because
381 they proved to yield the most indicative scores for tracking model errors or
382 improvement along the various intercomparison exercises (IPCC, 2013).

383

384 The drift is determined for either concentrations in simulated biogeochemical fields or
385 for skill score metrics (e.g., RMSE) using a linear regression fit over a time window
386 of 100 years. This time window of 100 years was chosen as a trade-off between a
387 longer time window (>200 years) that smoothes the drift signal and a shorter time
388 window (<100 years) that introduces fluctuations due to internal variability and hence
389 impacting the quality of the fit (see the assessment performed with the millennial-long
390 CMIP5 *piControl* simulation of IPSL-CM5A-LR in Figure S1).

391 The drift is assumed to decrease exponentially during the spin-up simulation and is
392 described by a simple drift model:

$$393 \quad drift(t) = drift(t = 0) \times \exp\left(-\frac{1}{\tau} t\right) \quad (1)$$

394 where τ is the relaxation time of the respective field at a given depth level. It
395 corresponds to the time required to nullify the drift.

396

397 Our analyses focus on the global distribution of nitrate (NO_3), dissolved oxygen (O_2)
398 and the difference between total alkalinity and dissolved inorganic carbon (Alk-DIC).

399 The latter serves as an approximation of carbonate ion concentration following Zeebe
400 and Wolf-Gladrow (2001). We use this approximation of the carbonate ion
401 concentration rather than its concentration, $[\text{CO}_3^{2-}]$, since the latter was poorly
402 assessed in CMIP5 reference papers and was not provided by a majority of ESMs.
403 These three biogeochemical tracers were chosen because (1) most current
404 biogeochemical models simulate Alk, DIC, NO_3 and O_2 prognostically and (2) they
405 are frequently used in state-of-the-art model performance assessment (e.g., Anav et
406 al., 2013; Bopp et al., 2013; Doney et al., 2009; Friedrichs et al., 2009; 2007; Stow et
407 al., 2009), and (3) DIC and Alk are both used as “master tracers” for the carbonate
408 system in the ocean biogeochemistry models (while $[\text{CO}_3^{2-}]$, e.g., is not explicitly
409 transported as a tracer with the velocity fields but diagnosed from temperature,
410 salinity, DIC, Alk, $[\text{H}^+]$, and pCO_2 when needed) . Modeled distributions of NO_3 , O_2
411 and Alk-DIC reflect the representation of biogeochemical processes related to the
412 biological pump (CO_2 , NO_3 , O_2), the air-sea gas exchange and ocean ventilation (CO_2
413 and O_2), as well as carbonate chemistry (Alk-DIC). These biogeochemical processes
414 are of particular relevance for investigating the impact of climate change on marine
415 productivity (e.g., Henson et al., 2010), ocean deoxygenation (e.g., Gruber, 2011;
416 Keeling et al., 2009) and the ocean carbon sink, processes for which future projections
417 with the current generation of ESMs yield large inter-model spreads (e.g.,
418 Friedlingstein et al., 2013; Resplandy et al., 2015; Séférian et al., 2014; Tjiputra et al.,
419 2014).

420

421 **3 Results**

422 **3-1 Comparison of observational datasets**

423 Our review of spin-up protocols for CMIP5 ESM shows that several modeling groups

424 have employed different streams of datasets to initialize their biogeochemical models
425 (e.g., WOA1994, WOA2001), while model evaluation relies on the most up-to-date
426 stream of data. Differences between the two data streams used for initializing and
427 assessing, respectively, NO_3 and O_2 concentrations are analyzed. Table 2 summarizes
428 RMSE and correlation between WOA1994 and WOA2013 for these two
429 biogeochemical fields.

430

431 Table 2 indicates that differences between the two streams of data are fairly small.
432 The total difference (RMSE) represents a departure between 5 to 10% from the global
433 average concentrations of WOA2013 across depth levels. It is generally lower in
434 regions where the sampling density has not increased markedly between the two
435 releases. These values can be used as a baseline for model-to-model comparison
436 assuming that errors attributed to the various sources of initialization cannot be larger
437 than 10%. Considering that some models have used outputs from previous model
438 simulations or globally averaged concentrations as initial conditions, we acknowledge
439 that this baseline is not a perfect criterion for benchmarking model performance.
440 There is, however, no ideal solution to address this issue since there is no standardized
441 set of initial conditions in CMIP5 except some recommendations for the decadal
442 prediction exercise in which specific attention was paid to initialization (e.g.,
443 Keenlyside et al., 2008; Kim et al., 2012; Matei et al., 2012; Meehl et al., 2013; 2009;
444 Servonnat et al., 2014; Smith et al., 2007; Swingedouw et al., 2013).

445

446 **3-2 Equilibration state metrics in IPSL-CM5A-LR**

447 The global mean sea surface temperature (SST) is a common metric to quantify the
448 energetic equilibrium of the model. This metric has been widely used in various

449 papers referenced in this study to determine the equilibration of ESM physical
450 components. Figure 2a shows the evolution of this metric during the 500-year long
451 spin-up simulation. The global average SST sharply decreases during the first 250
452 years of the simulation. In the last 250 years of the simulation, the global averaged
453 SST displays a small residual drift of $\sim 10^{-4} \text{ }^\circ\text{C y}^{-1}$ which falls into the range of the
454 drifts reported for CMIP5 ESMs (Sen Gupta et al., 2013). The evolution over the last
455 250 years is comparable to those of other physical equilibration metrics, such as the
456 ocean heat content or the meridional overturning circulation (Mignot et al., 2013).
457
458 To assess if ocean carbon cycle reservoirs are equilibrated, we track the temporal
459 evolution of sea-to-air CO₂ fluxes during the spin-up simulation. This metrics was
460 used in phase 2 of the Ocean Carbon Model Intercomparison Project (OCMIP-2, Orr
461 (2002)) and has still widely been used during CMIP5 as an equilibration metric for the
462 marine biogeochemistry. Figure 2b presents its evolution in the 500-year long spin-up
463 simulation. The global ocean sea-to-air CO₂ flux is $\sim -0.7 \text{ Pg C y}^{-1}$ over the last
464 decades of the spin-up simulation (negative values indicate ocean CO₂ uptake).
465 We use the range of values estimated from preindustrial natural ocean carbon flux
466 inversions (e.g. Gerber and Joos (2010) or Mikaloff Fletcher et al. (2007)) to evaluate
467 the global sea-to-air carbon flux simulated by IPSL-CM5A-LR. Since, these estimates
468 do not account for the preindustrial carbon outgassing induced by the river input,
469 while our model does, we have added a constant outgassing of 0.45 Pg C y^{-1} to the
470 range of $0.03 \pm 0.08 \text{ Pg C y}^{-1}$ (Mikaloff Fletcher et al. 2007). This value of 0.45 Pg C
471 y^{-1} corresponds to the global open-ocean river-induced carbon outgassing accordingly
472 to IPCC (2013) or Le Quéré et al. (2015). Consequently, in our modeling framework,
473 the target value of the global sea-to-air carbon flux ranges between 0.4 and 0.56 Pg C

474 y^{-1} .

475

476 Figure 2b shows that the global sea-to-air carbon flux is still lower than the range of
477 values estimated from preindustrial natural ocean carbon flux inversions (~ 0.4 - 0.56
478 $\text{Pg C } y^{-1}$). Besides, Figure 2b shows that the drift in the global sea-to-air carbon flux
479 becomes smaller more slowly after a strong decline during the first 50 years of the
480 spin-up simulation. From year 250-500 this drift is about $0.001 \text{ Pg C } y^{-2}$ and still
481 weaker over the last century of the simulation ($7 \times 10^{-4} \text{ Pg C } y^{-2}$). A one-sided t-test
482 indicates that the two drifts differ from each other with a p-value $< 2 \times 10^{-16}$. When
483 fitted with drifts computed from overlapping time segments of 100 years, our simple
484 drift model (Equation 1) gives a relaxation time of around 160 years. We use this
485 relaxation time and the drift of $7 \times 10^{-4} \text{ Pg C } y^{-2}$ to estimate the additional spin-up time
486 required for the model to reach an outgassing of 0.4 - $0.56 \text{ Pg C } y^{-1}$, as 1100 to 1300
487 years. However, even after this integration time, the drift in global sea-to-air carbon
488 flux estimated with our simple drift model still ranges from 2×10^{-7} to $7 \times 10^{-7} \text{ Pg C } y^{-2}$.
489

490 These estimates do not account for the non-linearity of the ocean carbon cycle and the
491 associated process uncertainties (Schwinger et al., 2014), and hence potentially
492 underestimate the time required to equilibrate the ocean carbon cycle and sea-to-air
493 carbon fluxes in the range of inversion estimates. The drift of $0.001 \text{ Pg C } y^{-2}$ is,
494 however, much smaller than the oceanic sink for anthropogenic carbon. Even if not
495 fully equilibrated in terms of carbon balance, it is likely that this run would have
496 given consistent estimates of anthropogenic carbon uptake in transient historical
497 hindcasts.

498

499 **3-3 Temporal evolution of model errors in IPSL-CM5A-LR**

500 Figure 3 shows the temporal evolution of globally averaged concentrations for O₂,
501 NO₃ and Alk-DIC at the surface (panels a, b and c), 150 m (panels d, e and f) and
502 2000 m (panels g, h, and i). Globally averaged concentrations of O₂, NO₃ and Alk-
503 DIC (solid lines) reach steady state after 100 to 250 years of spin-up at the surface.
504 While modeled nominal values for O₂ concentration converge toward the observed
505 concentration (i.e., 172.3 μmol L⁻¹), that of NO₃ presents persistent deviations from
506 WOA2013. At the surface, the convergence of the simulated oxygen to observed
507 value is expected since the dominant governing process of thermodynamic saturation
508 (through the air-sea gas exchange) is well understood and modeled. The deviation in
509 surface NO₃ highlights uncertainty related to near surface biological processes and
510 upper ocean physics. Below the surface, concentrations of biogeochemical tracers
511 drift away from the globally averaged concentrations computed from WOA2013 or
512 GLODAP (Figure 3, panels d-i). At 150 and 2000 meters, the drift in global averaged
513 concentrations for these fields, computed over the last 250 years, is still significant
514 with $p < 10^{-4}$ (Table 3). Except for the surface fields, Figure 3 shows that RMSE,
515 indicated with dashed lines in Figure 3, globally increases with time for all
516 biogeochemical fields. The linear drift in RMSE over the last 250 years of the spin-up
517 simulation falls within the 2-3 % ky⁻¹ range at the surface. It is much larger at 2000 m
518 (144-280 % ky⁻¹ ; Table 3). This is also the case regionally, because the latitudinal
519 maximum in RMSE (RMSE_{max}) is similar to the global RMSE. Table 3 also shows
520 that the magnitude of drift in RMSE for O₂, NO₃ and Alk-DIC differs at a given depth
521 as different processes affect the interior distribution of these biogeochemical fields.

522

523 **3-4 Evolution of geographical mismatches in IPSL-CM5A-LR**

524 To further explore the evolution of mismatch in biogeochemical distributions, we
525 analyze differences (ϵ) between simulated and observed fields of O_2 , NO_3 from
526 WOA2013 and Alk-DIC from GLODAP after the initialization and at the end of the
527 spin-up, i.e., the first year and the last year of the core spin-up simulation performed
528 with the IPSL-CM5A-LR model (Figures 4, 5 and 6).

529

530 Figure 4 (panels a, c, and e) shows that surface concentrations of biogeochemical
531 fields are associated with small biases at initialization. This error represents less than
532 5% of the observed surface concentrations for O_2 , NO_3 and Alk-DIC and reflects the
533 weak difference between the data stream employed for initialization and validation.
534 After 500 years of spin-up, deviations between the modeled and observed fields at the
535 surface have increased locally by up to ~40% (Figure 4, panels b, d, and f). The
536 largest deviations are found in high-latitude oceans for O_2 and NO_3 and also to some
537 extent in the tropics for NO_3 and Alk-DIC.

538

539 Below the surface, distributions of modeled biogeochemical fields compare well to
540 the observations at 150 m at initialization with averaged errors close to zero (Figure 5,
541 panels a, c, and e). This result was expected since WOA2013 and WOA1994 differ
542 little at these depth levels. Subsurface distributions at initialization strongly contrast
543 with the concentrations that resulted from 500 years of spin-up (Figure 5, panels b, d,
544 and f). After 500 years of spin-up, substantial mismatches characterize the distribution
545 of O_2 , NO_3 and Alk-DIC fields in the high-latitude oceans and in the tropics. Figure 5
546 illustrates that patterns of errors for O_2 , NO_3 and Alk-DIC fields are well correlated
547 with each other ($R > 0.6$). This reflects that in PISCES carbon, nitrogen and oxygen
548 concentrations are linked by the elemental C:N:- ΔO_2 stoichiometry fixed in space and

549 time. Figure 6 shows that model-data deviations at 2000 m have substantially
550 increased at a regional level after 500 years of simulation, showing large errors in the
551 Southern Hemisphere oceans. This appears clearly in Figure 6, panels d and f for NO_3
552 and Alk-DIC fields, respectively.

553

554 The temporal evolution of the RMSE between modeled and observed fields of O_2 ,
555 NO_3 and Alk-DIC over the whole water column is presented in Figure 7 in terms of
556 RMSE (Figure 7, panels a-c). As expected, Figure 7 illustrates that there is a good
557 match during the first years of simulation for all biogeochemical fields at all depth
558 levels with low RMSE. After a few centuries, patterns of error evolve differently
559 across depth for O_2 , NO_3 and Alk-DIC.

560 The temporal evolution of RMSE shows that patterns of error have reached a steady
561 state a few decades after 250 years of spin-up within the upper hundred meters of the
562 ocean but continue to evolve at greater depths, even after 500 years. Patterns of errors
563 within the thermocline and upper 1000 m water masses evolve relatively fast (within a
564 few centuries) due to the relatively short mixing time in the upper ocean. Mid-depth
565 (~1500-2500 m) RMSE evolves much slower because of the slow ocean circulation at
566 these depth levels. Characteristics time scales here are thousand of years as evidenced
567 by the observed radiocarbon age of seawater (e.g., Wunsch and Heimbach, 2007;
568 2008). This explains why, at the end of the spin-up simulation, two maxima of
569 comparable amplitude are found for RMSE at 150 m and 3750 m for O_2 and at 50 m
570 and 3800 m for Alk-DIC (Figure 7).

571

572 **3-5 Drifts in IPSL-CM5A-LR spin-up simulation**

573 With the evolution of the RMSE established, we can use the simple drift model

574 (Equation 1) to determine the relaxation time, τ , which characterizes the e-folding
575 time scale of the RMSE. To use this simple drift model, we compute the drift in
576 RMSE determined from time segments of 100 years distributed evenly every 5 years
577 from year 250 to 500 for O₂, NO₃ and Alk-DIC tracers. The drift model (magenta
578 lines in Figure 8) is fitted to the 80 drift values for each field and each depth level
579 (colored crosses in Figure 8).

580

581 The simple drift model fits well the evolution of the drift in RMSE for the
582 biogeochemical variables along the spin-up simulation of IPSL-CM5A-LR (Figure 8).
583 Correlation coefficients are mostly significant at 90% confidence level ($r^*=0.3$
584 determined with a student distribution with significance level of 90% and ~ 15
585 effective degrees of freedom estimated with the formulation of Bretherton et al.,
586 (1999)), except for NO₃ at surface and Alk-DIC at 150 m and 2000 m. Another
587 exception is found for NO₃ at 150 m where the drift does not correspond to an
588 exponential decay of the drift as function of time. The large confidence interval of the
589 fit indicates that the fit would have been considered as non-significant given a longer
590 spin-up simulation or a higher confidence threshold.

591

592 When significant, estimates of τ for O₂ RMSE are $\approx 90, 564$ and 1149 y at the surface
593 150 m and 2000 m, respectively. These values match reasonably well τ estimated for
594 NO₃ RMSE at 2000 m (1130 y) and those for Alk-DIC RMSE at surface and 2000 m
595 (137 and 1163 y). However, these estimates are sensitive to the time windows used to
596 compute the drift. For a subset of time windows between 100 and 250 years by step of
597 50 years, τ estimates for O₂ RMSE are $\approx 114\pm 67, 375\pm 140$ and 1116 ± 527 y at the
598 surface 150 m and 2000 m depth. These large uncertainties associated with τ

599 estimates are essentially due to the length of the spin-up simulation. A longer spin-up
600 simulation would improve the quality of the fit (see Figure S1).

601

602 **3-6 Drifts in CMIP5 ESMs preindustrial simulations**

603 In this subsection, the analysis is extended to the CMIP5 archive. We focus on oxygen
604 fields in the long preindustrial simulation, *piControl*, for the 15 available CMIP5
605 ESMs. From these simulations that span from 250 to 1000 years, we compute the drift
606 in O₂ RMSE across depth from several time segments of 100 years distributed evenly
607 every 5 years from the beginning until the end of the piControl simulation. These
608 drifts are used as a surrogate for drift computed from the spin-up of each model since
609 such simulations are not available through the data portal.

610

611 Figure 9 represents the drift in O₂ RMSE versus the spin-up duration for each CMIP5
612 ESM. The analysis shows that the drift in O₂ RMSE differs substantially between
613 models. For a given model, drifts in other biogeochemical tracers (NO₃ and Alk-DIC)
614 display similar features (not shown). The between-model differences in drift are not
615 surprising since there are no reasons for different models to exhibit similar drift for a
616 given field. Yet, Figure 9 shows that a global relationship emerges from this ensemble
617 when using the simple drift model to fit the drift in O₂ RMSE as function of the spin-
618 up duration (solid green lines in Figure 9). With a 90% confidence level, this
619 relationship suggests a general decrease of the drift as a function of spin-up duration
620 for all depth levels. At the surface and at 2000 m depth, the quality of fits is low with
621 correlation coefficients of about 0.4. These are however significant at 90%
622 confidence level ($r^*=0.34$ determined with a student distribution with significance
623 level of 90% and 15 models as degree of freedom). The weakest correlation

624 coefficient is found for the fit at 150 m depth and hence indicating that there is no link
625 between the drift in O₂ RMSE and the duration of the spin-up simulation. This low
626 significance level must be put into perspective given the large diversity of spin-up
627 protocols and initial conditions (Figure 1 and Table 1) that can deteriorate the drift-
628 spin up duration relationship in this ensemble of models.

629

630 The drift versus spin up duration relationship established from the 15 CMIP5 ESMs is
631 nonetheless consistent with the results obtained with IPSL-CM5A-LR (The results in
632 Figure 8 have been reported in Figure 9 with magenta crosses). Indeed, the drifts in
633 RMSE decreases in course of time at the various depth levels for the IPSL-CM5A-LR
634 model, although their magnitudes differ. This difference in magnitude is not
635 surprising if one considers that drift is highly model and protocol dependent and that
636 the length of the IPSL-CM5A-LR spin-up simulation is potentially too short to
637 determine accurate estimates of the long-term drift in O₂ RMSE. Despite these
638 differences, our analyses show that a relationship between the drift in O₂ RMSE
639 versus the spin-up duration emerges from an ensemble of models and is broadly
640 consistent with our theoretical framework of a drift model established from the results
641 of the IPSL-CM5A-LR model (Figure 8).

642

643 **3-7 Impact of the drift on model skill score assessment metrics across CMIP5**

644 **ESMs**

645 In the following, we investigate the influence of model drift on skill score assessment
646 metrics that are routinely used to benchmark model performance. For this purpose, we
647 use the ensemble-mean O₂ RMSE as a metrics to assess the distance between the
648 biogeochemical observations and model results. For this purpose, we compute O₂
649 RMSE from each ensemble member of the CMIP5 models averaged from 1986 to

650 2005 with respect to WOA2013 observations. The model-data distance is then
651 determined for each CMIP5 model using the mean across the available ensemble
652 members.

653

654 The left hand side panels of Figure 10 present the performance of available CMIP5
655 models in terms of distance to oxygen observations at the surface, 150 m and 2000 m,
656 respectively. In these panels, the various CMIP5 models are ordered as function of
657 their distance to the oxygen observations. Following Knutti et al. (2013), either the
658 ensemble mean or the ensemble median is used to identify groups of models with
659 similar skill within the CMIP5 ensemble. The left hand side panels of Figure 10 show
660 that the ability of models to reproduce oxygen observations varies across depth levels.
661 The RMSE in the simulated O₂ fields in CESM1-BGC, HadGEM2-ES, HadGEM2-
662 CC, GFDL-ESM2M, MPI-ESM-LR and MPI-ESM-MR is generally smaller than the
663 ensemble mean or ensemble median RMSE across the various depth levels (Figure 10
664 panels a, b and c). On the other side of the ranking, CMCC-CESM, CNRM-CM5,
665 CNRM-CM5-2, IPSL-CM5B-LR and NorESM1-ME exhibit RMSE generally higher
666 than the ensemble mean and median RMSE across the various depth levels. The other
667 models, i.e., CNRM-ESM1, GFDL-ESM2G, IPSL-CM5A-LR and IPSL-CM5A-MR
668 display O₂ RMSE that is generally close to the ensemble mean or the ensemble
669 median.

670

671 To assess the impact of model's drift inherited from the diversity of spin-up strategies
672 (Figure 1 and Table 1) on the performance metrics, we use a simple additive
673 assumption to incorporate an incremental error due to the drift, Δ RMSE, to the above-
674 mentioned RMSE. This incremental error due to the drift is computed using the

675 relaxation time τ determined from the *piControl* simulations of each CMIP5 model at
676 each depth level (Equation 1 and Figure 9) and a common duration of $T=3000$ years
677 for all models (m):

$$678 \quad \Delta RMSE_m(z) = \int_0^T drift_m(z, t = 0) \times \exp\left(-\frac{1}{\tau(z)} t\right) dt \quad (2)$$

679 where $\Delta RMSE$ has the same unit as RMSE.

680 The common duration T is used to bring model drift close to zero and hence to make
681 models comparable to each other.

682 We employ $\Delta RMSE$ to penalize the distance from the observations assuming that this
683 drift-induced deviation in tracer fields can be added to RMSE. This means that the
684 effect of the penalty is to increase the distance giving a consistent measure of the
685 equilibration error.

686

687 The right hand side panels of Figure 10 show the influence of this penalization
688 approach on the model ranking at the various depth levels. They show that several
689 models have been upgraded in the ranking while others have not. For example, both
690 MPI-ESM-LR, MPI-ESM-MR have been upgraded at the surface and 2000 m. On the
691 other hand, the rank of HadGEM2-ES and HadGEM2-CC has been downgraded to
692 the 5th and 3th position due to the large drift in surface oxygen concentrations in
693 comparison to that of the other models. The surface drift might be attributed to drivers
694 in oxygen fluxes (e.g., SST, SSS). The ranking of GFDL-ESM2G and GFDL-
695 ESM2M slightly changes with penalization but both models stay close to the
696 ensemble mean or the ensemble median. At the bottom of the ranking, models with
697 large deviation from the oxygen observations (i.e., CMCC-CESM, IPSL-CM5B-LR,
698 NorESM1-ME, CNRM-CM5) are found. For these models, the computed $\Delta RMSE$

699 and RMSE result in similar ranking, because even a small drift and hence relatively
700 low Δ RMSE cannot compensate for their large RMSE.

701

702 **4- Discussion**

703 **4-1 Implications for biogeochemical processes**

704 Our results show that errors in ocean biogeochemical fields amplify during the spin-
705 up simulation but not at the same rate at all depths. These differences in error
706 evolution are consistent with an increasing contribution of biogeochemical processes
707 in setting the distribution of tracers at depth. Indeed, Mignot et al. (2013) with the
708 same model simulation showed that the main physical climate fields as well as the
709 large-scale ocean circulation reach quasi-equilibrium after 250 years of spin-up, but
710 our analyses indicate that biogeochemical tracers do not (Figure 3).

711

712 Besides, our analysis demonstrates that drift in biogeochemical fields are highly
713 model dependent. For example, despite having the same initialization strategy and
714 comparable spin up duration, the GFDL-ESM2G, GFDL-ESM2M, and NorESM1-
715 ME models display considerable difference in drift (Figures 9 and 10) that mirror
716 large differences in model performance and properties (e.g., resolution, simulated
717 processes).

718

719 The identification of the dynamical or biogeochemical processes responsible for these
720 errors is not within the scope of this study and would required additional long
721 simulations with additional tracers targeted for attribution of the various
722 biogeochemical processes and the underlying ocean physics (e.g., Doney et al., 2004)
723 involved (e.g. using abiotic, passive tracers as suggested in Walin et al. (2014)). Some

724 mechanisms can be nonetheless invoked to explain differences or similarities in
725 behavior between biogeochemical fields. For example, the evolution of surface
726 concentrations for O₂ and Alk-DIC is controlled in part by the solubility of O₂ and
727 CO₂ in seawater and the concentration of these gases in the atmosphere (set to the
728 observed values and kept constant in all experiments performed with IPSL-CM5A-LR
729 discussed here) and the biological soft-tissue and calcium carbonate counter pumps
730 (in relation with the vertical transport of nutrients and alkalinity). Therefore, the
731 equilibration of the O₂ and Alk-DIC surface fields once the physical equilibrium is to
732 a large degree reached (~250 years of spin-up) is expected (Figure 3, panels a and c
733 and Figure 7). Nevertheless, spatial errors could increase depending on the physical
734 state of the model (Figure 4, panels b and f). By contrast, the evolution of NO₃
735 concentration is predominantly determined by ocean circulation, biological processes,
736 and to a lesser extent by external supplies from rivers and atmosphere. Below the
737 surface, concentrations of O₂, NO₃, and Alk-DIC evolve in response to the combined
738 effect of ocean circulation and biogeochemical processes. The combination of
739 dynamical and biogeochemical processes on the one hand, and the spin-up strategy on
740 the other hand both shape the modeled distributions of large-scale biogeochemical
741 tracers.

742

743 Consequences of the difficulty in achieving the correct equilibration procedure have
744 important implications for biogeochemical features that are defined by regional
745 characteristics in tracer concentrations, such as high nutrient/low chlorophyll regions,
746 oxygen minimum zones and nutrient-to-light colimitation patterns. This point is
747 illustrated by recent studies focusing on future changes in phytoplankton productivity
748 (e.g. Vancoppenolle et al. (2013) and Laufkötter et al. (2015). Vancoppenolle and co-

749 workers report a wide spread of surface mean NO₃ concentrations (1980-1999) in the
750 Arctic with a range from 1.7 to 8.9 μmol L⁻¹ across a subset of 11 CMIP5 models. The
751 spread in present day NO₃ concentrations translates into a large model-to-model
752 uncertainty in future net primary production. Laufkötter and colleagues determined
753 limitation terms of phytoplankton production for a subset of CMIP5 and MAREMIP
754 (Marine Ecosystem Model Intercomparison Project) models. The authors demonstrate
755 that nutrient-to-light colimitation patterns differ in strength, location and type between
756 models and arise from large differences in the simulated nutrient concentrations.
757 Although Vancoppenolle et al. (2013) and Laufkötter et al. (2015) explain a part of
758 the difference in simulated nutrient concentration by the differences in the spatial
759 resolution and the complexity of the models, the authors of both studies qualitatively
760 invoked differences in spin-up duration to explain the remaining differences in
761 simulated concentrations. Besides, a recent assessment of interannual to decadal
762 variability of ocean CO₂ and O₂ fluxes in CMIP5 models, suggests that decadal
763 variability can range regionally from 10 to 50% of the total natural variability among
764 a subset of 6 ESMs (Resplandy et al., 2015). In that study, the authors demonstrate
765 that, despite the robustness of driving mechanisms (mostly related to vertical transport
766 of water masses) across the model ensemble, model-to-model spread can be related to
767 differences in modeled carbon and oxygen concentrations. In light of present results,
768 it appears likely that differences in spin-up strategy and sources of initialization could
769 also contribute to the amplitude of the natural variability of the ocean CO₂ and O₂
770 fluxes.

771

772 **4-2 Implications for future projections**

773 The inconsistent strategies used to spin-up models in CMIP5 have resulted in a

774 significant source of uncertainty to the multi-model spread. It needs to be better
775 constrained in order to draw robust conclusions on the impact of climate change on
776 the carbon cycle as well as on climate feedback (e.g., Arora et al., 2013; Friedlingstein
777 et al., 2013; Roy et al., 2011; Schwinger et al., 2014; Séférian et al., 2012) and on
778 marine ecosystems (e.g., Bopp et al., 2013; Boyd et al., 2015; Cheung et al., 2012;
779 Doney et al., 2012; Gattuso et al., 2015; Lehodey et al., 2006). So far, the most
780 frequently used approach relies on long preindustrial control simulations running
781 parallel to a transient simulations, allowing the ‘removal’ of the drift in the simulated
782 fields over the historical period or future projections (e.g., Bopp et al., 2013; Cocco et
783 al., 2013; Friedlingstein et al., 2013; 2006; Frölicher et al., 2014; Gehlen et al., 2014;
784 Keller et al., 2014; Steinacher et al., 2010; Tjiputra et al., 2014). Although this
785 approach allows one to determine relative changes, it does not allow to investigate the
786 underlying reasons of the spread between models in terms of processes, variability
787 and response to climate change. The “drift-correction” approach, much as the one
788 used for this study, assumes that drift-induced errors in the simulated fields can be
789 isolated from the signal of interest. Verification of this fundamental hypothesis would
790 require a specific experimental set-up consisting of the perturbation of model fields
791 (e.g., nutrients or carbon-related fields) to assess by how much the model projections
792 would be modified. So far, several modeling groups have generated ensemble
793 simulation in CMIP5 using a perturbation approach. However, the perturbations were
794 applied either to physical fields only or to both the physical and marine
795 biogeochemical fields. To assess impacts of different spin-up strategies and/or initial
796 conditions on future projections of marine biogeochemical tracer distributions,
797 ensemble simulations in which only biogeochemical fields are perturbed would be
798 needed.

799

800 **4-3 Implications for multi-model skill-score assessments.**

801 While the importance of spin-up protocols is well accepted in the modeling
802 community, the link between spin-up strategy and the ability of a model to reproduce
803 modern observations remains to be addressed.

804

805 Most of the recent CMIP5 skill assessment approaches were based on *historical*
806 hindcasts that were started from preindustrial runs of varying duration and from
807 various spin-up strategies. Therefore, in typical intercomparison exercises, Earth
808 system models with a short spin-up, and hence modeled distributions still close to
809 initial fields, are confronted with Earth system models with a longer spin-up duration
810 and modeled distributions that have drifted further away from their initial states. Our
811 study highlights that such inconsistencies in spin-up protocols and initial conditions
812 across CMIP5 Earth system models (Figure 1 and Table 1) could significantly
813 contribute to model-to-model spread in performance metrics. The analysis of the first
814 century of CMIP5 *piControl* simulations demonstrated a significant spread of drift
815 between CMIP5 models (Figure 9). An approximate exponential relationship between
816 the amplitude of drift and the spin up duration emerges from the ensemble of CMIP5
817 models, which is consistent with results from IPSL-CM5A-LR. For example, while
818 the global average root-mean square error increased up to 70% during a 500-year
819 spin-up simulation with IPSL-CM5A-LR, its rate of increase (or drift) decreased with
820 time to a very small rate ($0.001 \text{ Pg C y}^{-1}$). Combining a simple drift model and this
821 relationship, we propose a penalization approach in an effort to assess more
822 objectively the influence of documented model differences on model-data biases.
823 Figure 10 compares the standard approach to assess model performance (left hand

824 side panels) to the drift-penalized approach (right hand side panels). This novel
825 approach penalizes models with larger drift without affecting the models with smaller
826 drift. Taking into account drift in modeled fields results in subtle adjustments in
827 ranking, which reflect differences in spin-up and initialization strategies.

828

829 **4-4 Limitations of the framework**

830 In this work, the analyses focus on the globally averaged O₂ RMSE across a diverse
831 ensemble of CMIP5 models, which differ in terms of represented processes, spatial
832 resolution and performance in addition to differences in spin-up protocols. Major
833 limitations of the framework are presented below.

834

835 Due to their specificities in terms of processes and resolution (e.g., Cabré et al.,
836 (2015), Laufkötter et al. (2015)), regional drift in CMIP5 models may differ from the
837 drift computed from globally averaged skill-score metrics (see Figure S2 and S3).
838 These differences may lead to different estimates of the relaxation time τ at regional
839 scale. Moreover, the combination of regional ocean physics and biogeochemical
840 processes in each individual model may drive an evolution of a regional drift in
841 RMSE that does not fit the hypothesis of an exponential decay of the drift during the
842 course of the spin-up simulation.

843

844 Besides, difference in the simulated processes and resolution in the different models
845 can explain the relatively low confidence level of the fit to drift across the multi-
846 model CMIP5 ensemble (Figure 9). The relatively low significance level of the fit
847 reflects not only the large diversity of spin-up protocols and initial conditions (Figure
848 1 and Table 1) but also the large diversity of processes and resolution of the CMIP5

849 models. Indeed, as shown in Kriest and Oschlies (2015), various parameterizations of
850 the particle sinking speed in a common physical framework may lead to a similar
851 evolution of the globally averaged RMSE in the first century of the spin-up simulation
852 but display very different behavior within a time-scale of $O(10^3)$ years. As such, drift
853 and τ estimates need to be used with caution when computed from short spin-up
854 simulations because they can be subject to large uncertainties. An improved
855 derivation of the penalization would require access to output from spin-up simulations
856 for each individual model or, at least, a better quantification of model-model
857 differences in terms of initial conditions.

858

859 **5- Conclusions and recommendation for future intercomparison exercises**

860 Skill-score metrics are expected to be widely used in the framework of the upcoming
861 CMIP6 (Meehl et al., 2014) with the development of international community
862 benchmarking tools like the ESMValTool (<http://www.pa.op.dlr.de/ESMValTool> , see
863 also Eyring et al. (2015)). The assessment of model skill to reproduce observations
864 will focus on the modern period. Complementary to this approach, our results call for
865 the consideration of spin-up and initialization strategies in the determination of skill
866 assessment metrics (e.g., Friedrichs et al., 2009; Stow et al., 2009) and, by extension,
867 to model weighting (e.g., Steinacher et al., 2010) and model ranking (e.g., Anav et al.,
868 2013). Indeed, the use of equilibrium-state metrics of the model like the 3-
869 dimensional drift of relevant skill score metrics (e.g. RMSE) could be employed to
870 increase the reliability of these traditional metrics and, as such, should be included in
871 the set of standard assessment tools for CMIP6.

872

873 In an effort to better represent interactions between marine biogeochemistry and

874 climate (Smith et al., 2014), future generations of Earth system models are likely to
875 include more complex ocean biogeochemical models, be it in terms of processes (e.g.,
876 Tagliabue and Völker, 2011; Tagliabue et al., 2011) or interactions with other
877 biogeochemical cycles (e.g., Gruber and Galloway, 2008) or increased spatial
878 resolution (e.g., Dufour et al., 2013; Lévy et al., 2012) in order to better represent
879 mesoscale biogeochemical dynamics. These developments will go along with an
880 increase in the diversity and complexity of spin-up protocols applied to Earth system
881 models, especially those including an interactive atmospheric CO₂ or interactive
882 nitrogen cycle (e.g., Dunne et al., 2013; Lindsay et al., 2014). The additional
883 challenge of spinning-up emission-driven simulations with interactive carbon cycle
884 will also require us to extend the assessment of the impact of spin-up protocols to the
885 terrestrial carbon cycle. Processes such as soil carbon accumulation, peat formation as
886 well as shift in biomes such as tropical and boreal ecosystems for dynamic vegetation
887 models require several long time-scales to equilibrate (Brovkin et al., 2010; Koven et
888 al., 2015). In addition, the terrestrial carbon cycle has large uncertainties in terms of
889 carbon sink/source behavior (Anav et al., 2013; Dalmonech et al., 2014; Friedlingstein
890 et al., 2013) which might affect ocean CO₂ uptake (Brovkin et al., 2010). A novel
891 numerical algorithm to accelerate the spin-up integration time for computationally
892 expensive ocean biogeochemical models has emerged (Khatiwala, 2008), which could
893 help to disentangle physical from biogeochemical contribution to the inter-model
894 spreads, but at the same time, could also potentially complicate the determination of
895 inter-model spreads by increasing the diversity of spin-up protocols.

896

897 To evaluate the contribution of variable spin-up and initialization strategies to model
898 performance, these should be documented extensively and the corresponding model

899 output should be archived. Ideally, for future coupled model intercomparison
900 exercises (i.e., CMIP6, CMIP7, Meehl et al., (2014)), the community should agree on
901 a set of simple recommendations for spin-up protocols, following past projects such
902 as OCMIP-2. In parallel, any trade-off between model equilibration and
903 computationally efficient spin-up procedures has to be linked with efforts to reduce
904 model errors due to the physical and biogeochemical parameterizations.

905

906

907 *Acknowledgement:*

908 *We sincerely thank I. Kriest, F. Joos, the anonymous reviewer and A Yool for*
909 *their useful comments on this paper. This work was supported by the H2020 project*
910 *CRESCENDO “Coordinated Research in Earth Systems and Climate : Experiments,*
911 *kNowledge, Dissemination and Outreach” which received funding from the European*
912 *Union’s Horizon 2020 research and innovation programme under grant agreement*
913 *No 641816 and by the EU FP7 project CARBOCHANGE “Changes in carbon uptake*
914 *and missions by oceans in a changing climate” which received funding from the*
915 *European community’s Seventh Framework Programme under grant agreement no.*
916 *264879. Supercomputing time was provided by GENCI (Grand Equipement National*
917 *de Calcul Intensif) at CCRT (Centre de Calcul Recherche et Technologie), allocation*
918 *016178. Finally, we are grateful to the ESGF project which makes data available for*
919 *all the community. R.S. is grateful Aurélien Ribes for his kind advices on statistics. JT*
920 *acknowledges ORGANIC project (239965/F20) funded by the Research Council of*
921 *Norway. CH and TJ are grateful for support through project EVA - Earth system*
922 *modelling of climate variations in the Anthropocene (229771/E10) funded by the*
923 *Research Council of Norway, as well as CPU-time and mass storage provided*
924 *through NOTUR project NN2345K as well as NorStore project NS2345K. K.L. and*
925 *S.C.D. acknowledge support from the National Science Foundation.*
926

927

928 *References:*

929 Adachi, Y., Yukimoto, S., Deushi, M., Obata, A., Nakano, H., Tanaka, T. Y., Hosaka,
930 M., Sakami, T., Yoshimura, H., Hirabara, M., Shindo, E., Tsujino, H., Mizuta, R.,
931 Yabu, S., Koshiro, T., Ose, T. and Kitoh, A.: Basic performance of a new earth
932 system model of the Meteorological Research Institute (MRI-ESM1), Papers in
933 Meteorology and Geophysics, 64, 1–18, doi:10.2467/mripapers.64.1, 2013.

934 Anav, A., Friedlingstein, P., Kidston, M., Bopp, L., Ciais, P., Cox, P., Jones, C., Jung,

- 935 M., Myneni, R. and Zhu, Z.: Evaluating the Land and Ocean Components of the
 936 Global Carbon Cycle in the CMIP5 Earth System Models, *J. Climate*, 26(18), 6801–
 937 6843, doi:10.1175/JCLI-D-12-00417.1, 2013.
- 938 Andrews, O. D., Bindoff, N. L., Halloran, P. R., Ilyina, T. and Le Qu 'er 'e, C.:
 939 Detecting an external influence on recent changes in oceanic oxygen using an optimal
 940 fingerprinting method, *Biogeosciences*, 10(3), 1799–1813, doi:10.5194/bg-10-1799-
 941 2013, 2013.
- 942 Archer, D., Buffett, B. and Brovkin, V.: Ocean methane hydrates as a slow tipping
 943 point in the global carbon cycle, *Proceedings of the National Academy of Sciences*,
 944 106(49), 20596–20601, 2009.
- 945 Arora, V. K., Boer, G. J., Friedlingstein, P., Eby, M., Jones, C. D., Christian, J. R.,
 946 Bonan, G., Bopp, L., Brovkin, V., Cadule, P., Hajima, T., Ilyina, T., Lindsay, K.,
 947 Tjiputra, J. F. and Wu, T.: Carbon–Concentration and Carbon–Climate Feedbacks in
 948 CMIP5 Earth System Models, *J. Climate*, 26(15), 5289–5314, doi:10.1175/JCLI-D-
 949 12-00494.1, 2013.
- 950 Arora, V. K., Scinocca, J. F., Boer, G. J., Christian, J. R., Denman, K. L., Flato, G.
 951 M., Kharin, V. V., Lee, W. G. and Merryfield, W. J.: Carbon emission limits required
 952 to satisfy future representative concentration pathways of greenhouse gases, *Geophys.*
 953 *Res. Lett.*, 38(5), L05805, doi:10.1029/2010GL046270, 2011.
- 954 Aumont, O. and Bopp, L.: Globalizing results from ocean in situ iron fertilization
 955 studies, *Global Biogeochem. Cycles*, 20(2), GB2017, doi:10.1029/2005GB002591,
 956 2006.
- 957 Aumont, O., Maier-Reimer, E., Blain, S. and Monfray, P.: An ecosystem model of the
 958 global ocean including Fe, Si, P colimitations, *Global Biogeochem. Cycles*, 17(2),
 959 1060, doi:10.1029/2001GB001745, 2003.
- 960 Aumont, O., Orr, J. C., Monfray, P., Ludwig, W., Amiotte-Suchet, P. and Probst, J.-
 961 L.: Riverine-driven interhemispheric transport of carbon, *Global Biogeochem. Cycles*,
 962 15(2), 393–405, doi:10.1029/1999GB001238, 2001.
- 963 Aumont, O., Orr, J., Jamous, D., Monfray, P., Marti, O. and Madec, G.: A degradation
 964 approach to accelerate simulations to steady-state in a 3-D tracer transport model of
 965 the global ocean, *Climate Dynamics*, 14(2), 101–116, 1998.
- 966 Bopp, L., Resplandy, L., Orr, J. C., Doney, S. C., Dunne, J. P., Gehlen, M., Halloran,
 967 P., Heinze, C., Ilyina, T., Séférian, R., Tjiputra, J. and Vichi, M.: Multiple stressors of
 968 ocean ecosystems in the 21st century: projections with CMIP5 models,
 969 *Biogeosciences*, 10(10), 6225–6245, doi:10.5194/bg-10-6225-2013, 2013.
- 970 Boyd, P. W., Lennartz, S. T., Glover, D. M. and Doney, S. C.: Biological
 971 ramifications of climate-change-mediated oceanic multi-stressors, *Nature Clim.*
 972 *Change*, 5(1), 71–79, 2015.
- 973 Bretherton, C. S., Widmann, M., Dymnikov, V. P., Wallace, J. M. and Bladé, I.: The
 974 Effective Number of Spatial Degrees of Freedom of a Time-Varying Field, *J. Climate*,

- 975 12(7), 1990–2009, doi:10.1175/1520-0442(1999)012<1990:TENOSD>2.0.CO;2,
976 1999.
- 977 Brovkin, V., Lorenz, S. J., Jungclaus, J., Raddatz, T., Timmreck, C., Reick, C. H.,
978 Segschneider, J. and Six, K.: Sensitivity of a coupled climate-carbon cycle model to
979 large volcanic eruptions during the last millennium, *Tellus B*, 62(5), 674–681,
980 doi:10.1111/j.1600-0889.2010.00471.x, 2010.
- 981 Bryan, K.: Accelerating the Convergence to Equilibrium of Ocean-Climate Models, *J.*
982 *Phys. Oceanogr.*, 14(4), 666–673, doi:10.1175/1520-
983 0485(1984)014<0666:ATCTEO>2.0.CO;2, 1984.
- 984 Cheung, W. W. L., Sarmiento, J. L., Dunne, J. P., Frölicher, T. L., Lam, V. W. Y.,
985 Palomares, M. L. D., Watson, R. and Pauly, D.: Shrinking of fishes exacerbates
986 impacts of global ocean changes on marine ecosystems, *Nature Climate change*,
987 2(10), 1–5, doi:10.1038/nclimate1691, 2012.
- 988 Cabré, A., Marinov, I., Bernardello, R. and Bianchi, D.: Oxygen minimum zones in
989 the tropical Pacific across CMIP5 models: mean state differences and climate change
990 trends, *Biogeosciences*, 12(18), 5429–5454, doi:10.5194/bg-12-5429-2015, 2015.
- 991 Cocco, V., Joos, F., Steinacher, M., Frölicher, T. L., Bopp, L., Dunne, J., Gehlen, M.,
992 Heinze, C., Orr, J., Oschlies, A., Schneider, B., Segschneider, J. and Tjiputra, J.:
993 Oxygen and indicators of stress for marine life in multi-model global warming
994 projections, *Biogeosciences*, 10(3), 1849–1868, doi:10.5194/bg-10-1849-2013, 2013.
- 995 Collins, W. J., Bellouin, N., Doutriaux-Boucher, M., Gedney, N., Halloran, P.,
996 Hinton, T., Hughes, J., Jones, C. D., Joshi, M., Liddicoat, S., Martin, G., O'Connor,
997 F., Rae, J., Senior, C., Sitch, S., Totterdell, I., Wiltshire, A. and Woodward, S.:
998 Development and evaluation of an Earth-System model – HadGEM2, *Geosci. Model*
999 *Dev*, 4(4), 1051–1075, doi:10.5194/gmd-4-1051-2011, 2011.
- 1000 Cox, P. M., Pearson, D., Booth, B. B., Friedlingstein, P., Huntingford, C., Jones, C. D.
1001 and Luke, C. M.: Sensitivity of tropical carbon to climate change constrained by
1002 carbon dioxide variability, *Nature*, 494(7437), 341–344, doi:10.1038/nature11882,
1003 2013.
- 1004 Dalmonech, D., Foley, A. M., Anav, A., Friedlingstein, P., Friend, A. D., Kidston, M.,
1005 Willeit, M. and Zaehle, S.: Challenges and opportunities to reduce uncertainty in
1006 projections of future atmospheric CO₂: a combined marine and terrestrial biosphere
1007 perspective, *Biogeosciences Discuss.*, 11(2), 2083–2153, doi:10.5194/bgd-11-2083-
1008 2014, 2014.
- 1009 de Baar, H. J. W. and de Jong, J. T. M.: *The biogeochemistry of iron in seawater*,
1010 edited by D. R. Turner and K. A. Hunter, John Wiley, Hoboken, N. J., 2001.
- 1011 Doney, S. C., Lindsay, K., Caldeira, K., Campin, J.-M., Drange, H., Dutay, J.-C.,
1012 Follows, M., Gao, Y., Gnanadesikan, A., Gruber, N., Ishida, A., Joos, F., Madec, G.,
1013 Maier-Reimer, E., Marshall, J. C., Matear, R. J., Monfray, P., Mouchet, A., Najjar, R.,
1014 Orr, J. C., Plattner, G.-K., Sarmiento, J., Schlitzer, R., Slater, R., Totterdell, I. J.,
1015 Weirig, M.-F., Yamanaka, Y. and Yool, A.: Evaluating global ocean carbon models:

- 1016 The importance of realistic physics, *Global Biogeochem. Cycles*, 18(3),
1017 doi:10.1029/2003GB002150, 2004.
- 1018 Doney, S. C.: The Growing Human Footprint on Coastal and Open-Ocean
1019 Biogeochemistry, *Science*, 328(5985), 1512–1516, doi:10.1126/science.1185198,
1020 2010.
- 1021 Doney, S. C., Lima, I., Moore, J. K., Lindsay, K., Behrenfeld, M. J., Westberry, T. K.,
1022 Mahowald, N., Glover, D. M. and Takahashi, T.: Skill metrics for confronting global
1023 upper ocean ecosystem-biogeochemistry models against field and remote sensing
1024 data, *Journal of Marine Systems*, 76(1-2), 95–112,
1025 doi:10.1016/j.jmarsys.2008.05.015, 2009.
- 1026 Doney, S. C., Ruckelshaus, M., Emmett Duffy, J., Barry, J. P., Chan, F., English, C.
1027 A., Galindo, H. M., Grebmeier, J. M., Hollowed, A. B., Knowlton, N., Polovina, J.,
1028 Rabalais, N. N., Sydeman, W. J. and Talley, L. D.: Climate Change Impacts on
1029 Marine Ecosystems, *Annu. Rev. Marine. Sci.*, 4(1), 11–37, doi:10.1146/annurev-
1030 marine-041911-111611, 2012.
- 1031 Dufour, C. O., Sommer, J. L., Gehlen, M., Orr, J. C., Molines, J.-M., Simeon, J. and
1032 Barnier, B.: Eddy compensation and controls of the enhanced sea-to-air CO₂ flux
1033 during positive phases of the Southern Annular Mode, *Global Biogeochem. Cycles*,
1034 27(3), 950–961, doi:10.1002/gbc.20090, 2013.
- 1035 Dufresne, J.-L., Foujols, M. A., Denvil, S., Caubel, A., Marti, O., Aumont, O.,
1036 Balkanski, Y., Bekki, S., Bellenger, H., Benshila, R., Bony, S., Bopp, L., Braconnot,
1037 P., Brockmann, P., Cadule, P., Cheruy, F., Codron, F., Cozic, A., Cugnet, D., Noblet,
1038 N., Duvel, J. P., Ethe, C., Fairhead, L., Fichefet, T., Flavoni, S., Friedlingstein, P.,
1039 Grandpeix, J. Y., Guez, L., Guilyardi, E., Hauglustaine, D., Hourdin, F., Idelkadi, A.,
1040 Ghattas, J., Joussaume, S., Kageyama, M., Krinner, G., Labetoulle, S., Lahellec, A.,
1041 Lefebvre, M.-P., Lefèvre, F., Lévy, C., Li, Z. X., Lloyd, J., Lott, F., Madec, G.,
1042 Mancip, M., Marchand, M., Masson, S., Meurdesoif, Y., Mignot, J., Musat, I.,
1043 Parouty, S., Polcher, J., Rio, C., Schulz, M., Swingedouw, D., Szopa, S., Talandier,
1044 C., Terray, P., Viovy, N. and Vuichard, N.: Climate change projections using the
1045 IPSL-CM5 Earth System Model: from CMIP3 to CMIP5, *Clim Dyn*, 40(9-10), 2123–
1046 2165, doi:10.1007/s00382-012-1636-1, 2013.
- 1047 Dunne, J. P., John, J. G., Adcroft, A. J., Griffies, S. M., Hallberg, R. W., Shevliakova,
1048 E., Stouffer, R. J., Cooke, W., Dunne, K. A., Harrison, M. J., Krasting, J. P.,
1049 Malyshev, S. L., Milly, P. C. D., Philipps, P. J., Sentman, L. A., Samuels, B. L.,
1050 Spelman, M. J., Winton, M., Wittenberg, A. T. and Zadeh, N.: GFDL’s ESM2 Global
1051 Coupled Climate–Carbon Earth System Models. Part I: Physical Formulation and
1052 Baseline Simulation Characteristics, *J. Climate*, 25(19), 6646–6665, doi:doi:
1053 10.1175/JCLI-D-11-00560.1, 2013.
- 1054 Duplessy, J. C., Bard, E., Arnold, M., Shackleton, N. J., Duprat, J. and Labeyrie, L.:
1055 How fast did the ocean–atmosphere system run during the last deglaciation? *Earth
1056 and Planetary Science Letters*, 103(1-4), 27–40, doi:10.1016/0012-821X(91)90147-A,
1057 1991.
- 1058 Eyring, V., Righi, M., Evaldsson, M., Lauer, A., Wenzel, S., Jones, C., Anav, A.,

- 1059 Andrews, O., Cionni, I., Davin, E. L., Deser, C., Ehbrecht, C., Friedlingstein, P.,
1060 Gleckler, P., Gottschaldt, K. D., Hagemann, S., Jukes, M., Kindermann, S., Krasting,
1061 J., Kunert, D., Levine, R., Loew, A., Mäkelä, J., Martin, G., Mason, E., Phillips, A.,
1062 Read, S., Rio, C., Roehrig, R., Senftleben, D., Sterl, A., van Ulft, L. H., Walton, J.,
1063 Wang, S. and Williams, K. D.: ESMValTool (v1.0) – a community diagnostic and
1064 performance metrics tool for routine evaluation of Earth System Models in CMIP,
1065 *Geosci. Model Dev. Discuss.*, 8(9), 7541–7661, 2015.
- 1066 Fichetfet, T. and Maqueda, M. A. M.: Sensitivity of a global sea ice model to the
1067 treatment of ice thermodynamics and dynamics, *J. Geophys. Res.*, 102(C6), 12609–
1068 12646, 1997.
- 1069 Follows, M. J., Dutkiewicz, S., Grant, S. and Chisholm, S. W.: Emergent
1070 Biogeography of Microbial Communities in a Model Ocean, *Science*, 315(5820),
1071 1843–1846, doi:10.1126/science.1138544, 2007.
- 1072 Friedlingstein, P., Cox, P., Betts, R., Bopp, L., Bloh, Von, W., Brovkin, V., Cadule,
1073 P., Doney, S., Eby, M., Fung, I., Bala, G., John, J., Jones, C., Joos, F., Kato, T.,
1074 Kawamiya, M., Knorr, W., Lindsay, K., Matthews, H. D., Raddatz, T., Rayner, P.,
1075 Reick, C., Roeckner, E., Schnitzler, K. G., Schnur, R., Strassmann, K., Weaver, A. J.,
1076 Yoshikawa, C. and Zeng, N.: Climate–Carbon Cycle Feedback Analysis: Results from
1077 the C 4MIP Model Intercomparison, *J. Climate*, 10(14), 3337–3353,
1078 doi:10.1175/JCLI3800.1, 2006.
- 1079 Friedlingstein, P., Meinshausen, M., Arora, V. K., Jones, C. D., Anav, A., Liddicoat,
1080 S. K. and Knutti, R.: Uncertainties in CMIP5 climate projections due to carbon cycle
1081 feedbacks, *J. Climate*, 130917124100006, doi:doi: 10.1175/JCLI-D-12-00579.1,
1082 2013.
- 1083 Friedrichs, M. A. M., Carr, M.-E., Barber, R. T., Scardi, M., Antoine, D., Armstrong,
1084 R. A., Asanuma, I., Behrenfeld, M. J., Buitenhuis, E. T., Chai, F., Christian, J. R.,
1085 Ciotti, A. M., Doney, S. C., Dowell, M., Dunne, J. P., Gentili, B., Gregg, W.,
1086 Hoepffner, N., Ishizaka, J., Kameda, T., Lima, I., Marra, J., Mélin, F., Moore, J. K.,
1087 Morel, A., O'Malley, R. T., O'Reilly, J., Saba, V. S., Schmeltz, M., Smyth, T. J.,
1088 Tjiputra, J., Waters, K., Westberry, T. K. and Winguth, A.: Assessing the
1089 uncertainties of model estimates of primary productivity in the tropical Pacific Ocean,
1090 *Journal of Marine Systems*, 76(1-2), 113–133, doi:10.1016/j.jmarsys.2008.05.010,
1091 2009.
- 1092 Friedrichs, M. A. M., Dusenberry, J. A., Anderson, L. A., Armstrong, R. A., Chai, F.,
1093 Christian, J. R., Doney, S. C., Dunne, J. P., Fujii, M., Hood, R., McGillicuddy, D. J.,
1094 Jr., Moore, J. K., Schartau, M., Spitz, Y. H. and Wiggert, J. D.: Assessment of skill
1095 and portability in regional marine biogeochemical models: Role of multiple
1096 planktonic groups, *J. Geophys. Res.*, 112(C8), doi:10.1029/2006JC003852, 2007.
- 1097 Frölicher, T. L., Sarmiento, J. L., Paynter, D. J., Dunne, J. P., Krasting, J. P. and
1098 Winton, M.: Dominance of the Southern Ocean in anthropogenic carbon and heat
1099 uptake in CMIP5 models, *J. Climate*, 141031131835005, doi:10.1175/JCLI-D-14-
1100 00117.1, 2014.
- 1101 Gattuso, J. P., Magnan, A., Bille, R., Cheung, W. W. L., Howes, E. L., Joos, F.,

- 1102 Allemand, D., Bopp, L., Cooley, S. R., Eakin, C. M., Hoegh-Guldberg, O., Kelly, R.
 1103 P., Portner, H. O., Rogers, A. D., Baxter, J. M., Laffoley, D., Osborn, D., Rankovic,
 1104 A., Rochette, J., Sumaila, U. R., Treyer, S. and Turley, C.: Contrasting futures for
 1105 ocean and society from different anthropogenic CO₂ emissions scenarios, *Science*,
 1106 349(6243), aac4722–aac4722, doi:10.1126/science.aac4722, 2015.
- 1107 Gehlen, M., Séférian, R., Jones, D. O. B., Roy, T., Roth, R., Barry, J., Bopp, L.,
 1108 Doney, S. C., Dunne, J. P., Heinze, C., Joos, F., Orr, J. C., Resplandy, L.,
 1109 Segschneider, J. and Tjiputra, J.: Projected pH reductions by 2100 might put deep
 1110 North Atlantic biodiversity at risk, *Biogeosciences*, 11(23), 6955–6967, 2014.
- 1111 Gerber, M. and Joos, F.: Carbon sources and sinks from an Ensemble Kalman Filter
 1112 ocean data assimilation - Gerber - 2010 - *Global Biogeochemical Cycles* - Wiley
 1113 Online Library, *Global Biogeochem. Cycles*, 24, GB3004,
 1114 doi:[10.1029/2009GB003531](https://doi.org/10.1029/2009GB003531), 2010.
- 1115 Gnanadesikan, A.: Oceanic ventilation and biogeochemical cycling: Understanding
 1116 the physical mechanisms that produce realistic distributions of tracers and
 1117 productivity, *Global Biogeochem. Cycles*, 18(4), doi:10.1029/2003GB002097, 2004.
- 1118 Gruber, N.: Warming up, turning sour, losing breath: ocean biogeochemistry under
 1119 global change, *Philosophical Transactions of the Royal Society A: Mathematical,*
 1120 *Physical and Engineering Sciences*, 369(1943), 1980–1996,
 1121 doi:10.1098/rsta.2011.0003, 2011.
- 1122 Gruber, N. and Galloway, J. N.: An Earth-system perspective of the global nitrogen
 1123 cycle, *Nature*, 451(7176), 293–296, doi:doi:10.1038/nature06592, 2008.
- 1124 Sen Gupta, A. S., Muir, L. C., Brown, J. N., Phipps, S. J., Durack, P. J., Monselesan,
 1125 D. and Wijffels, S. E.: Climate Drift in the CMIP3 Models, *J. Climate*, 25(13), 4621–
 1126 4640, doi:10.1175/JCLI-D-11-00312.1, 2012.
- 1127 Sen Gupta, A. S., Jourdain, N. C., Brown, J. N. and Monselesan, D.: Climate Drift in
 1128 the CMIP5 models, *J. Climate*, 26(21), 8597–8615. <http://doi.org/10.1175/JCLI-D-12-00521.s1>.
 1129
- 1130 Hajima, T., Kawamiya, M., Watanabe, M., Kato, E., Tachiiri, K., Sugiyama, M.,
 1131 Watanabe, S., Okajima, H. and Ito, A.: Modeling in Earth system science up to and
 1132 beyond IPCC AR5, *Progress in Earth and Planetary Science*, 1(1), 29–25,
 1133 doi:10.1186/s40645-014-0029-y, 2014.
- 1134 Heinze, C., Maier-Reimer, E., Winguth, A. and Archer, D.: A global oceanic sediment
 1135 model for long-term climate studies, *Global Biogeochem. Cycles*, 13(1), 221–250,
 1136 1999.
- 1137 Heinze, M. and Ilyina, T.: Ocean biogeochemistry in the warm climate of the late
 1138 Paleocene, *Climate of the Past*, 11(1), 1933–1975, doi:10.5194/cp-11-63-2015, 2015.
- 1139 Henson, S. A., Sarmiento, J. L., Dunne, J. P., Bopp, L., Lima, I., Doney, S. C., John,
 1140 J. and Beaulieu, C.: Detection of anthropogenic climate change in satellite records of
 1141 ocean chlorophyll and productivity, *Biogeosciences*, 7(2), 621–640, doi:10.5194/bg-7-621-2010, 2010.

- 1143 Hobbs, W., Palmer, M. D. and Monselesan, D.: An Energy Conservation Analysis of
 1144 Ocean Drift in the CMIP5 Global Coupled Models: *Journal of Climate*: Vol 29, No 5,
 1145 *J. Climate*, 29(5), 1639–1653, doi:10.1175/JCLI-D-15-0477.s1, 2015.
- 1146 Hourdin, F., Musat, I., Bony, S., Braconnot, P., Codron, F., Dufresne, J.-L., Fairhead,
 1147 L., Filiberti, M.-A., Friedlingstein, P., Grandpeix, J.-Y., Krinner, G., LeVan, P., Li,
 1148 Z.-X. and Lott, F.: The LMDZ4 general circulation model: climate performance and
 1149 sensitivity to parametrized physics with emphasis on tropical convection, *Climate*
 1150 *Dynamics*, 27, 787–813, doi:10.1007/s00382-006-0158-0, 2006.
- 1151 Ilyina, T., Six, K. D., Segschneider, J., Maier-Reimer, E., Li, H. and Núñez-Riboni, I.:
 1152 Global ocean biogeochemistry model HAMOCC: Model architecture and
 1153 performance as component of the MPI-Earth system model in different CMIP5
 1154 experimental realizations, *J. Adv. Model. Earth Syst.*, 5(2), 287–315,
 1155 doi:10.1029/2012MS000178, 2013.
- 1156 IPCC: *Climate Change 2013: The Physical Science Basis*, edited by: Stoker, T. F.,
 1157 Qin, D., Plattner, G., Tignor, M., Allen, S. K., Boschung, J., Nauels, A., Xia, Y.,
 1158 Bex, V., and Midgley, P. M., Cambridge Univ. Press, Cambridge, UK, and New
 1159 York, NY, USA, 2013..
- 1160 Ito, T. and Deutsch, C.: Variability of the Oxygen Minimum Zone in the Tropical
 1161 North Pacific during the Late 20th Century, *Global Biogeochem. Cycles*, n/a–n/a,
 1162 doi:10.1002/2013GB004567, 2013.
- 1163 Ito, T., Woloszyn, M. and Mazloff, M.: Anthropogenic carbon dioxide transport in the
 1164 Southern Ocean driven by Ekman flow, *Nature*, 463(7277), 80–83,
 1165 doi:10.1038/nature08687, 2010.
- 1166 Jickells, T. and Spokes, L.: *The biogeochemistry of iron in seawater*, edited by D. R.
 1167 Turner and K. A. Hunter, John Wiley, Hoboken, N. J., 2001.
- 1168 Johnson, K., Chavez, F. and Friederich, G.: Continental-shelf sediment as a primary
 1169 source of iron for coastal phytoplankton, *Nature*, 398(6729), 697–700, 1999.
- 1170 Keeling, R. F., Körtzinger, A. and Gruber, N.: Ocean Deoxygenation in a Warming
 1171 World, *Annu. Rev. Marine. Sci.*, 2(1), 199–229,
 1172 doi:10.1146/annurev.marine.010908.163855, 2009.
- 1173 Keenlyside, N. S., Latif, M., Jungclaus, J., Kornblueh, L. and Roeckner, E.:
 1174 Advancing decadal-scale climate prediction in the North Atlantic sector, *Nature*,
 1175 453(7191), 84–88, doi:10.1038/nature06921, 2008.
- 1176 Keller, K. M., Joos, F. and Raible, C. C.: Time of emergence of trends in ocean
 1177 biogeochemistry, *Biogeosciences*, 11(13), 3647–3659, doi:10.5194/bgd-10-18065-
 1178 2013, 2014.
- 1179 Key, R., Kozyr, A., Sabine, C., Lee, K., Wanninkhof, R., Bullister, J., Feely, R.,
 1180 Millero, F., Mordy, C. and Peng, T.: A global ocean carbon climatology: Results from
 1181 Global Data Analysis Project (GLODAP), *Global Biogeochem. Cycles*, 18(4),
 1182 doi:10.1029/2004GB002247, 2004.

- 1183 Khatiwala, S., Visbeck, M. and Cane, M. A.: Accelerated simulation of passive
1184 tracers in ocean circulation models, *Ocean Modelling*, 9(1), 51–69,
1185 doi:10.1016/j.ocemod.2004.04.002, 2005.
- 1186 Khatiwala, S.: Fast spin up of ocean biogeochemical models using matrix-free
1187 Newton-Krylov, *Ocean Modelling*, 23, 121–129, 2008.
- 1188 Kim, H.-M., Webster, P. J. and Curry, J. A.: Evaluation of short-term climate change
1189 prediction in multi-model CMIP5 decadal hindcasts, *Geophys. Res. Lett.*, 39(10),
1190 L10701, doi:10.1029/2012GL051644, 2012.
- 1191 Knutti, R., Masson, D. and Gettelman, A.: Climate model genealogy: Generation
1192 CMIP5 and how we got there, *Geophys. Res. Lett.*, 40(6), 1194–1199,
1193 doi:10.1002/grl.50256, 2013.
- 1194 Koven, C. D., Chambers, J. Q., Georgiou, K., Knox, R., Negron-Juarez, R., Riley, W.
1195 J., Arora, V. K., Brovkin, V., Friedlingstein, P. and Jones, C. D.: Controls on
1196 terrestrial carbon feedbacks by productivity vs. turnover in the CMIP5 Earth System
1197 Models, *Biogeosciences Discuss.*, 12(8), 5757–5801, 2015.
- 1198 Kriest, I. and Oschlies, A.: MOPS-1.0: towards a model for the regulation of the
1199 global oceanic nitrogen budget by marine biogeochemical processes, *Geosci. Model
1200 Dev.*, 8(9), 2929–2957, doi:10.5194/gmd-8-2929-2015, 2015.
- 1201 Krinner, G., Viovy, N., de Noblet-Ducoudré, N., Ogée, J., Polcher, J., Friedlingstein,
1202 P., Ciais, P., Sitch, S. and Prentice, I. C.: A dynamic global vegetation model for
1203 studies of the coupled atmosphere-biosphere system, *Global Biogeochem. Cycles*,
1204 19(1), 1–33, 2005.
- 1205 Laufkötter, C., Vogt, M., Gruber, N., Aita-Noguchi, M., Aumont, O., Bopp, L.,
1206 Buitenhuis, E., Doney, S. C., Dunne, J., Hashioka, T., Hauck, J., Hirata, T., John, J.,
1207 Le Quéré, C., Lima, I. D., Nakano, H., Séférian, R., Totterdell, I., Vichi, M. and
1208 Völker, C.: Drivers and uncertainties of future global marine primary production in
1209 marine ecosystem models, *Biogeosciences*, 12(23), 6955–6984, 2015.
- 1210 Le Quéré, C., Moriarty, R., Andrew, R. M., Peters, G. P., Ciais, P., Friedlingstein, P.,
1211 Jones, S. D., Sitch, S., Tans, P., Arneeth, A., Boden, T. A., Bopp, L., Bozec, Y.,
1212 Canadell, J. G., Chini, L. P., Chevallier, F., Cosca, C. E., Harris, I., Hoppema, M.,
1213 Houghton, R. A., House, J. I., Jain, A. K., Johannessen, T., Kato, E., Keeling, R. F.,
1214 Kitidis, V., Klein Goldewijk, K., Koven, C., Landa, C. S., Landschützer, P., Lenton,
1215 A., Lima, I. D., Marland, G., Mathis, J. T., Metzl, N., Nojiri, Y., Olsen, A., Ono, T.,
1216 Peng, S., Peters, W., Pfeil, B., Poulter, B., Raupach, M. R., Regnier, P., Rödenbeck,
1217 C., Saito, S., Salisbury, J. E., Schuster, U., Schwinger, J., Séférian, R., Segschneider,
1218 J., Steinhoff, T., Stocker, B. D., Sutton, A. J., Takahashi, T., Tilbrook, B., van der
1219 Werf, G. R., Viovy, N., Wang, Y. P., Wanninkhof, R., Wiltshire, A. and Zeng, N.:
1220 Global carbon budget 2014, *Earth Syst. Sci. Data*, 7(1), 47–85, doi:10.5194/essd-7-
1221 47-2015, 2015.
- 1222 Lehodey, P., Alheit, J. and Barange, M.: Climate variability, fish, and fisheries,
1223 *Journal of Climate*, 2006.

- 1224 Levitus, S. and Boyer, T.: World ocean atlas 1994, volume 4: Temperature, PB--95-
1225 270112/XAB, National Environmental Satellite, Data, and Information Service,
1226 Washington, DC (United States). 1994.
- 1227 Levitus, S., Antonov, J. I., Baranova, O. K., Boyer, T. P., Coleman, C. L., Garcia,
1228 H. E., Grod- sky, A. I., Johnson, D. R., Locarnini, R. A., Mishonov, A. V., Reagan, J.
1229 R., Sazama, C. L., Seidov, D., Smolyar, I., Yarosh, E. S., and Zweng, M. M.: The
1230 World Ocean Database TI, Data Science Journal, 12, WDS229–WDS234, 2013.
- 1231 Levitus, S., Conkright, M. E., Reid, J. L., Najjar, R. G. and Mantyla, A.: Distribution
1232 of nitrate, phosphate and silicate in the world oceans, Progress in Oceanography,
1233 31(3), 245–273, 1993.
- 1234 Lévy, M., Lengaigne, M., Bopp, L., Vincent, E. M., Madec, G., Ethe, C., Kumar, D.
1235 and Sarma, V. V. S. S.: Contribution of tropical cyclones to the air-sea CO₂ flux: A
1236 global view, Global Biogeochem. Cycles, 26(2), doi:10.1029/2011GB004145, 2012.
- 1237 Lindsay, K., Bonan, G. B., Doney, S. C., Hoffman, F. M., Lawrence, D. M., Long, M.
1238 C., Mahowald, N. M., Moore, J. K., Randerson, J. T. and Thornton, P. E.:
1239 Preindustrial Control and 20th Century Carbon Cycle Experiments with the Earth
1240 System Model CESM1(BGC), J. Climate, 141006111735008, doi:10.1175/JCLI-D-
1241 12-00565.1, 2014a.
- 1242 Ludwig, W., Probst, J. and Kempe, S.: Predicting the oceanic input of organic carbon
1243 by continental erosion, Global Biogeochem. Cycles, 10(1), 23–41, 1996.
- 1244 Madec, G.: NEMO ocean engine, Institut Pierre-Simon Laplace (IPSL), France.
1245 Institut Pierre-Simon Laplace (IPSL). [online] Available from: [http://www.nemo-
1246 ocean.eu/About-NEMO/Reference-manuals](http://www.nemo-ocean.eu/About-NEMO/Reference-manuals), (last access: Novem- ber 2013) 2008.
- 1247 Maier-Reimer, E.: Geochemical cycles in an ocean general circulation model.
1248 Preindustrial tracer distributions, Global Biogeochem. Cycles, 7(3), 645,
1249 doi:10.1029/93GB01355, 1993.
- 1250 Maier-Reimer, E. and Hasselmann, K.: Transport and storage of CO₂ in the ocean —
1251 —an inorganic ocean-circulation carbon cycle model, Clim Dyn, 2(2), 63–90–90,
1252 doi:10.1007/BF01054491, 1987.
- 1253 Marinov, I., Gnanadesikan, A., Sarmiento, J. L., Toggweiler, J. R., Follows, M. and
1254 Mignone, B. K.: Impact of oceanic circulation on biological carbon storage in the
1255 ocean and atmospheric pCO₂, Global Biogeochem. Cycles, 22(3), GB3007,
1256 doi:10.1029/2007GB002958, 2008.
- 1257 Massonnet, F., Fichet, T., Goosse, H., Bitz, C. M., Philippon-Berthier, G., Holland,
1258 M. M. and Barriat, P. Y.: Constraining projections of summer Arctic sea ice, The
1259 Cryosphere, 6(6), 1383–1394, doi:10.5194/tc-6-1383-2012, 2012.
- 1260 Matei, D., Baehr, J., Jungclaus, J. H., Haak, H., Muller, W. A. and Marotzke, J.:
1261 Multiyear Prediction of Monthly Mean Atlantic Meridional Overturning Circulation at
1262 26.5 N, Science, 335(6064), 76–79, doi:10.1126/science.1210299, 2012.
- 1263 Meehl, G. A., Goddard, L., Boer, G., Burgman, R., Branstator, G., Cassou, C., Corti,

- 1264 S., Danabasoglu, G., Doblas-Reyes, F., Hawkins, E., Karspeck, A., Kimoto, M.,
 1265 Kumar, A., Matei, D., Mignot, J., Msadek, R., Pohlmann, H., Rienecker, M., Rosati,
 1266 T., Schneider, E., Smith, D., Sutton, R., Teng, H., van Oldenborgh, G. J., Vecchi, G.
 1267 and Yeager, S.: Decadal Climate Prediction: An Update from the Trenches, *Bull.*
 1268 *Amer. Meteor. Soc.*, doi:doi: 10.1175/BAMS-D-12-00241.1, 2013.
- 1269 Meehl, G. A., Goddard, L., Murphy, J., Stouffer, R. J., Boer, G., Danabasoglu, G.,
 1270 Dixon, K., Giorgetta, M. A., Greene, A. M., Hawkins, E., Hegerl, G., Karoly, D.,
 1271 Keenlyside, N., Kimoto, M., Kirtman, B., Navarra, A., Pulwarty, R., Smith, D.,
 1272 Stammer, D. and Stockdale, T.: Decadal Prediction, *Bull. Amer. Meteor. Soc.*, 90(10),
 1273 1467–1485, doi:10.1175/2009BAMS2778.1, 2009.
- 1274 Meehl, G. A., Moss, R., Taylor, K. E., Eyring, V., Stouffer, R. J., Bony, S. and
 1275 Stevens, B.: Climate Model Intercomparisons: Preparing for the Next Phase, *Eos*
 1276 *Trans. AGU*, 95(9), 77–78, doi:10.1002/2014EO090001, 2014.
- 1277 Mignot, J., Swingedouw, D., Deshayes, J., Marti, O., Talandier, C., S  ferian, R.,
 1278 Lengaigne, M. and Madec, G.: On the evolution of the oceanic component of the
 1279 IPSL climate models from CMIP3 to CMIP5: A mean state comparison, *Ocean*
 1280 *Modelling*, 72 IS -(0 SP - EP - PY - T2 -), 167–184, 2013.
- 1281 Mikaloff Fletcher, S. E., Gruber, N., Jacobson, A. R., Gloor, M., Doney, S. C.,
 1282 Dutkiewicz, S., Gerber, M., Follows, M., Joos, F., Lindsay, K., Menemenlis, D.,
 1283 Mouchet, A., M  ller, S. A. and Sarmiento, J. L.: Inverse estimates of the oceanic
 1284 sources and sinks of natural CO₂ and the implied oceanic carbon transport, *Global*
 1285 *Biogeochem. Cycles*, 21(1), GB1010, doi:10.1029/2006GB002751, 2007.
- 1286 Moore, J., Doney, S. and Lindsay, K.: Upper ocean ecosystem dynamics and iron
 1287 cycling in a global three-dimensional model, *Global Biogeochem. Cycles*, 18(4), –,
 1288 doi:10.1029/2004GB002220, 2004.
- 1289 Moore, J., Doney, S., Kleypas, J., Glover, D. and Fung, I.: An intermediate
 1290 complexity marine ecosystem model for the global domain, *Deep Sea Research Part*
 1291 *II: Topical Studies in Oceanography*, 49, 403–462, 2002.
- 1292 Orr, J. C.: *Global Ocean Storage of Anthropogenic Carbon*, Gif-sur-Yvette, France.
 1293 2002.
- 1294 Phillips, T. J., Potter, G. L., Williamson, D. L., Cederwall, R. T., Boyle, J. S., Fiorino,
 1295 M., Hnilo, J. J., Olson, J. G., Xie, S. and Yio, J. J.: Evaluating Parameterizations in
 1296 General Circulation Models: Climate Simulation Meets Weather Prediction, *Bull.*
 1297 *Amer. Meteor. Soc.*, 85(12), 1903–1915, doi:10.1175/BAMS-85-12-1903, 2004.
- 1298 Resplandy, L., Bopp, L., Orr, J. C. and Dunne, J. P.: Role of mode and intermediate
 1299 waters in future ocean acidification: Analysis of CMIP5 models, *Geophys. Res. Lett.*,
 1300 40(12), 3091–3095, 2013.
- 1301 Resplandy, L., S  ferian, R. and Bopp, L.: Natural variability of CO₂ and O₂ fluxes:
 1302 What can we learn from centuries-long climate models simulations? *Journal of*
 1303 *Geophysical Research-Oceans*, 120(1), 384–404, doi:10.1002/2014JC010463, 2015.
- 1304 Rodgers, K. B., Lin, J. and Fr  licher, T. L.: Emergence of multiple ocean ecosystem

- 1305 drivers in a large ensemble suite with an earth system model, *Biogeosciences*
 1306 *Discuss.*, 11(12), 18189–18227, doi:10.5194/bgd-11-18189-2014, 2014.
- 1307 Romanou, A., Gregg, W. W., Romanski, J. and Kelley, M.: Natural air–sea flux of
 1308 CO₂ in simulations of the NASA-GISS climate model: Sensitivity to the physical
 1309 ocean model formulation, *Ocean Modelling*, 66 IS -, 26–44,
 1310 doi:10.1016/j.ocemod.2013.01.008, 2013.
- 1311 Romanou, A., J. Romanski, and W.W. Gregg, 2014: Natural ocean carbon cycle
 1312 sensitivity to parameterizations of the recycling in a climate model. *Biogeosciences*,
 1313 11, 1137-1154, doi:10.5194/bg-11-1137-2014.
 1314
- 1315 Romanou, A., W.W. Gregg, J. Romanski, M. Kelley, R. Bleck, R. Healy, L.
 1316 Nazarenko, G. Russell, G.A. Schmidt, S. Sun, and N. Tausnev, 2013: Natural air-sea
 1317 flux of CO₂ in simulations of the NASA-GISS climate model: Sensitivity to the
 1318 physical ocean model formulation. *Ocean Model.*, 66, 26-44,
 1319 doi:10.1016/j.ocemod.2013.01.008.
- 1320 Rose, K. A., Roth, B. M. and Smith, E. P.: Skill assessment of spatial maps for
 1321 oceanographic modeling, *Journal of Marine Systems*, 76(1-2), 34–48,
 1322 doi:10.1016/j.jmarsys.2008.05.013, 2009.
- 1323 Roy, T., Bopp, L., Gehlen, M., Schneider, B., Cadule, P., Frölicher, T. L.,
 1324 Segsneider, J., Tjiputra, J., Heinze, C. and Joos, F.: Regional Impacts of Climate
 1325 Change and Atmospheric CO₂ on Future Ocean Carbon Uptake: A Multimodel Linear
 1326 Feedback Analysis, *J. Climate*, 24(9), 2300–2318, doi:10.1175/2010JCLI3787.1,
 1327 2011.
- 1328 Sarmiento, J. L. and Gruber, N.: *Ocean Biogeochemical Dynamics*, Princeton
 1329 University Press, Princeton, New Jersey, USA, 526 pp., 2006.
- 1330 Schwinger, J., Tjiputra, J. F., Heinze, C., Bopp, L., Christian, J. R., Gehlen, M.,
 1331 Ilyina, T., Jones, C. D., Salas-Mélia, D., Segsneider, J., Séférian, R. and Totterdell,
 1332 I.: Nonlinearity of Ocean Carbon Cycle Feedbacks in CMIP5 Earth System Models, *J.*
 1333 *Climate*, 27(11), 3869–3888, doi:10.1175/JCLI-D-13-00452.1, 2014.
- 1334 Servonnat, J., Mignot, J., Guilyardi, E., Swingedouw, D., Séférian, R. and Labetoulle,
 1335 S.: Reconstructing the subsurface ocean decadal variability using surface nudging in a
 1336 perfect model framework, *Clim Dyn*, 44(1-2), 1–24–24, doi:10.1007/s00382-014-
 1337 2184-7, 2014.
- 1338 Séférian, R., Bopp, L., Gehlen, M., Orr, J., Ethé, C., Cadule, P., Aumont, O., Salas y
 1339 Mélia, D., Voltaire, A. and Madec, G.: Skill assessment of three earth system models
 1340 with common marine biogeochemistry, *Climate Dynamics*, 40(9-10), 2549–2573,
 1341 doi:10.1007/s00382-012-1362-8, 2013.
- 1342 Séférian, R., Iudicone, D., Bopp, L., Roy, T. and Madec, G.: Water Mass Analysis of
 1343 Effect of Climate Change on Air–Sea CO₂ Fluxes: The Southern Ocean, *J. Climate*,
 1344 25(11), 3894–3908, doi:10.1175/JCLI-D-11-00291.1, 2012.
- 1345 Séférian, R., Ribes, A. and Bopp, L.: Detecting the anthropogenic influences on recent

- 1346 changes in ocean carbon uptake, *Geophys. Res. Lett.*, 2014GL061223,
1347 doi:10.1002/2014GL061223, 2014.
- 1348 S  f  rian, R., Delire, C., Decharme, B., Voldoire, A., Salas y M  lia, D., Chevallier,
1349 M., Saint-Martin, D., Aumont, O., Calvet, J.-C., Carrer, D., Douville, H.,
1350 Franchist  guy, L., Joetzjer, E. and S  n  si, S.: Development and evaluation of CNRM
1351 Earth-System model – CNRM-ESM1, *Geosci. Model Dev. Discuss.*, 8(7), 5671–5739,
1352 2015.
- 1353 Smith, D. M., Cusack, S., Colman, A. W., Folland, C. K., Harris, G. R. and Murphy,
1354 J. M.: Improved Surface Temperature Prediction for the Coming Decade from a
1355 Global Climate Model, *Science*, 317(5839), 796–799, doi:10.1126/science.1139540,
1356 2007.
- 1357 Smith, M. J., Palmer, P. I., Purves, D. W., Vanderwel, M. C., Lyutsarev, V.,
1358 Calderhead, B., Joppa, L. N., Bishop, C. M. and Emmott, S.: Changing how Earth
1359 System Modelling is done to provide more useful information for decision making,
1360 science and society, *Bull. Amer. Meteor. Soc.*, 140224132934008,
1361 doi:10.1175/BAMS-D-13-00080.1, 2014.
- 1362 Steinacher, M., Joos, F., Fr  licher, T. L., Bopp, L., Cadule, P., Cocco, V., Doney, S.
1363 C., Gehlen, M., Lindsay, K., Moore, J. K., Schneider, B. and Segschneider, J.:
1364 Projected 21st century decrease in marine productivity: a multi-model analysis,
1365 *Biogeosciences*, 7(3), 979–1005, doi:10.5194/bg-7-979-2010, 2010.
- 1366 Stouffer, R. J., Weaver, A. J. and Eby, M.: A method for obtaining pre-twentieth
1367 century initial conditions for use in climate change studies, *Clim Dyn*, 23(3-4), 327–
1368 339, doi:10.1007/s00382-004-0446-5, 2004.
- 1369 Stow, C. A., Jolliff, J., McGillicuddy, D. J. J., Doney, S. C., Allen, J. I., Friedrichs, M.
1370 A. M., Rose, K. A. and Wallhead, P.: Skill assessment for coupled biological/physical
1371 models of marine systems, *Journal of Marine Systems*, 76, 4–15,
1372 doi:10.1016/j.jmarsys.2008.03.011, 2009.
- 1373 Swingedouw, D., Mignot, J., Labetoulle, S., Guilyardi, E. and Madec, G.:
1374 Initialisation and predictability of the AMOC over the last 50 years in a climate
1375 model, *Clim Dyn*, 40(9-10), 2381–2399, doi:10.1007/s00382-012-1516-8, 2013.
- 1376 Tagliabue, A. and V  lker, C.: Towards accounting for dissolved iron speciation in
1377 global ocean models, *Biogeosciences*, 8(10), 3025–3039, 2011.
- 1378 Tagliabue, A., Bopp, L. and Gehlen, M.: The response of marine carbon and nutrient
1379 cycles to ocean acidification: Large uncertainties related to phytoplankton
1380 physiological assumptions, *Global Biogeochem. Cycles*, 25(3), GB3017–n/a,
1381 doi:10.1029/2010GB003929, 2011.
- 1382 Takahashi, T., Broecker, W. and Langer, S.: Redfield Ratio Based on Chemical-Data
1383 From Isopycnal Surfaces, *Journal of Geophysical Research-Oceans*, 90, 6907–6924,
1384 1985.
- 1385 Tanhua, T., Koertzienger, A., Friis, K., Waugh, D. W. and Wallace, D. W. R.: An

- 1386 estimate of anthropogenic CO₂ inventory from decadal changes in oceanic carbon
1387 content, *P Natl Acad Sci Usa*, 104(9), 3037–3042, doi:10.1073/pnas.0606574104,
1388 2007.
- 1389 Tegen, I. and Fung, I.: Contribution to the Atmospheric Mineral Aerosol Load From
1390 Land-Surface Modification, *J Geophys Res-Atmos*, 100, 18707–18726, 1995.
- 1391 Tjiputra, J. F., Olsen, A., Bopp, L., Lenton, A., Pfeil, B., Roy, T., Segschneider, J.,
1392 Totterdell, I. and Heinze, C.: Long-term surface pCO₂ trends from observations and
1393 models, *Tellus B; Vol 66 (2014)*, 66(2-3), 151–168, doi:10.1007/s00382-007-0342-x,
1394 2014.
- 1395 Tjiputra, J. F., Roelandt, C., Bentsen, M., Lawrence, D. M., Lorentzen, T., Schwinger,
1396 J., Seland, Ø. and Heinze, C.: Evaluation of the carbon cycle components in the
1397 Norwegian Earth System Model (NorESM), *Geosci. Model Dev*, 6(2), 301–325,
1398 doi:10.5194/gmd-6-301-2013, 2013.
- 1399 Vancoppenolle, M., Bopp, L., Madec, G., Dunne, J. P., Ilyina, T., Halloran, P. R. and
1400 Steiner, N.: Future Arctic Ocean primary productivity from CMIP5 simulations:
1401 Uncertain outcome, but consistent mechanisms, *Global Biogeochem. Cycles*, 27(3),
1402 605–619, 2013.
- 1403 Vichi, M., Manzini, E., Fogli, P. G., Alessandri, A., Patara, L., Scoccimarro, E.,
1404 Masina, S. and Navarra, A.: Global and regional ocean carbon uptake and climate
1405 change: sensitivity to a substantial mitigation scenario, *Climate Dynamics*, 37(9-10),
1406 1929–1947, doi:10.1007/s00382-011-1079-0, 2011.
- 1407 Volodin, E. M., Dianskii, N. A. and Gusev, A. V.: Simulating present-day climate
1408 with the INMCM4.0 coupled model of the atmospheric and oceanic general
1409 circulations, *Izv. Atmos. Ocean. Phys.*, 46(4), 414–431,
1410 doi:10.1134/S000143381004002X, 2010.
- 1411 Walin, G., Hieronymus, J. and Nycander, J.: Source-related variables for the
1412 description of the oceanic carbon system, *Geochem. Geophys. Geosyst.*, 15(9), 3675–
1413 3687, doi:10.1002/2014GC005383, 2014.
- 1414 Wanninkhof, R.: A relationship between wind speed and gas exchange over the ocean,
1415 *J. Geophys. Res.*, 97(C5), 7373–7382, 1992.
- 1416 Wassmann, P., Duarte, C. M., AGUSTÍ, S. and SEJR, M. K.: Footprints of climate
1417 change in the Arctic marine ecosystem, *Global Change Biol*, 17(2), 1235–1249,
1418 doi:10.1111/j.1365-2486.2010.02311.x, 2010.
- 1419 Watanabe, S., Hajima, T., Sudo, K., Nagashima, T., Takemura, T., Okajima, H.,
1420 Nozawa, T., Kawase, H., Abe, M., Yokohata, T., Ise, T., Sato, H., Kato, E., Takata,
1421 K., Emori, S. and Kawamiya, M.: MIROC-ESM 2010: model description and basic
1422 results of CMIP5-20c3m experiments, *Geosci. Model Dev*, 4(4), 845–872,
1423 doi:10.5194/gmdd-4-1063-2011, 2011.
- 1424 Wenzel, S., Cox, P. M., Eyring, V. and Friedlingstein, P.: Emergent constraints on
1425 climate-carbon cycle feedbacks in the CMIP5 Earth system models, *J. Geophys. Res.*
1426 *Biogeosci.*, 2013JG002591, doi:10.1002/2013JG002591, 2014.

1427 Wu, T., Li, W., Ji, J., Xin, X., Li, L., Wang, Z., Zhang, Y., Li, J., Zhang, F., Wei, M.,
1428 Shi, X., Wu, F., Zhang, L., Chu, M., Jie, W., Liu, Y., Wang, F., Liu, X., Li, Q., Dong,
1429 M., Liang, X., Gao, Y. and Zhang, J.: Global carbon budgets simulated by the Beijing
1430 Climate Center Climate System Model for the last century, *J Geophys Res-Atmos*,
1431 118(10), 4326–4347, doi:10.1002/jgrd.50320, 2013.

1432 Wunsch, C. and Heimbach, P.: Practical global oceanic state estimation, *Physica D:
1433 Nonlinear Phenomena*, 230(1-2), 197–208, doi:10.1016/j.physd.2006.09.040, 2007.

1434 Wunsch, C. and Heimbach, P.: How long to oceanic tracer and proxy equilibrium?
1435 *Quaternary Science Reviews*, 27(7-8), 637–651, doi:10.1016/j.quascirev.2008.01.006,
1436 2008.

1437 Yool, A., Oschlies, A., Nurser, A. J. G. and Gruber, N.: A model-based assessment of
1438 the TrOCA approach for estimating anthropogenic carbon in the ocean,
1439 *Biogeosciences*, 7(2), 723–751, 2010.

1440 Yool, A., Popova, E. E. and Anderson, T. R.: MEDUSA-2.0: an intermediate
1441 complexity biogeochemical model of the marine carbon cycle for climate change and
1442 ocean acidification studies, *Geosci. Model Dev*, 6(5), 1767–1811, doi:10.5194/gmd-6-
1443 1767-2013-supplement, 2013.

1444 Zeebe, R. E. and Wolf-Gladrow, D. A.: *CO₂ in seawater: equilibrium, kinetics,*
1445 *isotopes*, Elsevier Science Ltd. 2001.

1446

1447

1448

1449

1450

1451

1452

1453

1454

1455

1456

1457

1458

1459

1460

1461

1462

1463

Models	spin-up procedure	initial conditions	offline time	online time	total spin-up duration	References
BCC-CSM1-1	sequential	WOA2001, GLODAP	200	100	300	(Wu et al., 2013)
BCC-CSM1-1-m	sequential	WOA2001, GLODAP	200	100	300	(Wu et al., 2013)
CanESM2	sequential (forced w/ obs.)	OCMIP profiles, CanESM1	6000	600	6600	(Arora et al., 2011)
CESM1-BGC	direct	CCSM4	0	1000	1000	(Lindsay et al., 2014)
CMCC-CESM	sequential (w/ acc.)	WOA2001, GLODAP	100	100	200	(Vichi et al., 2011)
CNRM-CM5	sequential	WOA1994, GLODAP, IPSL	3000	100	3100	(Séférian et al., 2013)
CNRM-CM5-2	sequential	WOA1994, GLODAP, CNRM	3000	100	3100	(Schwinger et al., 2014)
CNRM-ESM1	sequential	CNRM-CM5	0	1300	1300	(Séférian et al., 2015)
GFDL-ESM2G	direct	WOA2005, GLODAP	0	1000	1000	(Dunne et al., 2013)
GFDL-ESM2M	direct	WOA2005, GLODAP	0	1000	1000	(Dunne et al., 2013)
GISS-E2-H-CC	direct	WOA2005, GLODAP DIC*	0	3300	3300	(Romanou et al., 2013)
GISS-E2-R-CC	direct	WOA2005, GLODAP DIC*	0	3300	3300	(Romanou et al., 2013)
HadGEM2-CC	sequential	HadCM3LC, WOA2011	400	100	500	(Collins et al., 2011; Wassmann et al., 2010)
HadGEM2-ES	sequential	HadCM3LC, WOA2010	400	100	500	(Collins et al., 2011)
INMCM4	sequential	Uniform DIC	3000	200	3200	(Volodin et al., 2010)
IPSL-CM5A-LR	sequential	WOA1994, GLODAP,	3000	600	3600	(Séférian et al., 2013)

		IPSL				
IPSL-CM5A-MR	sequential	WOA1994, GLODAP, IPSL	3000	300	3300	(Dufresne et al., 2013)
IPSL-CM5B-LR	sequential	IPSL- CM5A-LR	0	300	300	(Dufresne et al., 2013)
MIROC-ESM	sequential	GLODAP/c onstant values	1245	480	1725	(Watanabe et al., 2011)
MIROC-ESM- CHEM	sequential	GLODAP/c onstant values	1245	484	1729	(Watanabe et al., 2011)
MPI-ESM-LR	sequential	HAMOCC/ constant values	10000	1900	11900	(Ilyina et al., 2013)
MPI-ESM-MR	sequential	HAMOCC/ constant values	10000	1500	11500	(Ilyina et al., 2013)
MRI-ESM1	sequential (forced w/ obs.)	GLODAP	550	395	945	(Adachi et al., 2013)
NorESM	direct	WOA2010, GLODAP	0	900	900	(Tjiputra et al., 2013)

1464

1465 **Table 1:** Summary of spin-up strategy, sources of initial conditions, offline/online
1466 durations and references used to equilibrate ocean biogeochemistry in CMIP5 ESMs.
1467 The so-called direct and sequential strategies inform whether the spin-up of the ocean
1468 biogeochemical model is run directly in online/coupled mode or first in offline (ocean
1469 biogeochemistry only) and then in online/coupled mode. DIC* refers to the
1470 observation-derived estimates of preindustrial dissolved inorganic carbon
1471 concentration using the ΔC^* method. w/ acc. and forced w/ obs. indicates the strategy
1472 using ‘acceleration’ and observed atmospheric forcings during the spin-up,
1473 respectively.

1474

1475

	O ₂	NO ₃
--	----------------	-----------------

Depth	surface	150 m	2000 m	surface	150 m	2000 m
RMSE	7.19	8.75	5.50	2.07	2.90	2.08
R ²	0.98	0.98	0.99	0.96	0.92	0.94

1476

1477 **Table 2:** Differences between the oxygen (O₂, μmol L⁻¹) and nitrate (NO₃, μmol L⁻¹)

1478 datasets used for initializing IPSL-CM5A-LR (WOA1994) and the datasets used for

1479 assessing its performances (WOA2013).

1480

1481

	O ₂			NO ₃			Alk-DIC		
metrics	mean	RMSE	RMSE _{max}	mean	RMSE	RMSE _{max}	mean	RMSE	RMSE _{max}
Surf									
	-0.2	2.6	55.8	-0.1	-0.1	34.2	1.6	-0.1	-0.1
150 m									
	3.4	39.0	31.5	-15.9	33.4	55.2	6.1	27.9	24.7
2000 m									
	-30.4	144.3	-40.1	2	51.8	-34.8	-69.6	281.8	47.5

1482 **Table 3:** Drift in % ky⁻¹ for oxygen (O₂), nitrate (NO₃) and total alkalinity minus DIC

1483 (Alk-DIC) at surface, 150 and 2000 meters as simulated by the IPSL-CM5A-LR

1484 model. The drift has been computed over the last 250 years of the spin-up simulation

1485 using a linear regression fit of the globally averaged concentrations, root-mean

1486 squared error (RMSE) and latitudinal maximum root-mean squared error (RMSE_{max})

1487 with respect to the values at year 250.

1488

1489

1490

1491 **Figure 1:** Spin-up protocols of CMIP5 Earth system models. Color shading represents
1492 strategies of the various modeling groups. *Online* and *Offline* steps refer to runs
1493 performed with coupled climate model and with stand-alone ocean biogeochemistry
1494 model, respectively. Sources of initial conditions for biogeochemical component of
1495 CMIP5 Earth system models are indicated as hatching below the barplot.

1496

1497 **Figure 2:** Time series of two climate indices over the 500-year spin-up simulation of
1498 IPSL-CM5A-LR. They represent the global averaged sea surface temperature (a) and
1499 the global mean sea-air carbon flux (b). For sea-air carbon flux, negative value
1500 indicates uptake of carbon. Steady state equilibrium of physical components as
1501 described in Mignot et al., (2013) is reached at ~250 years and is indicated with a
1502 vertical dashed line. Drifts in sea surface temperature and global carbon flux are
1503 indicated with dashed blue lines. They are computed using a linear regression fit over
1504 years 250 to 500. Hatching on panel (b) represents the range of inverse modeling
1505 estimates for preindustrial global carbon flux as described in Mikaloff Fletcher et al.,
1506 (2007), i.e., $0.03 \pm 0.08 \text{ Pg C y}^{-1}$ plus 0.45 Pg C y^{-1} corresponding to the riverine-
1507 induced natural CO_2 outgassing outside of near-shore regions consistently with Le
1508 Quéré et al. (2015).

1509

1510 **Figure 3:** Time series of globally averaged concentration (in solid lines) and globally
1511 averaged root-mean squared error (RMSE in dashed lines) for dissolved oxygen (O_2),
1512 nitrate (NO_3) and difference between alkalinity and dissolved inorganic carbon (Alk-
1513 DIC) as simulated by IPSL-CM5A-LR. Globally averaged concentration and RMSE
1514 are given at surface (a,b and c), 150 m (d, e and f), and 2000 m (g, h and i) for these
1515 three biogeochemical fields. Their values are indicated on the left-side and right-side
1516 y-axis, respectively. Hatching represents the $\pm\sigma$ observational uncertainty due to
1517 optimal interpolation of in situ concentrations around the observed globally averaged
1518 concentration.

1519

1520 **Figure 4:** Snap-shots of spatial biases, ϵ , in surface concentrations ($\mu\text{mol L}^{-1}$) in
1521 biogeochemical fields during the 500-year spin-up simulation of IPSL-CM5A-LR. ϵ
1522 in dissolved oxygen (O_2), nitrate (NO_3) and difference between alkalinity and

1523 dissolved inorganic carbon (Alk-DIC) is given for the first year (a, c and e,
1524 respectively) and for the last year of spin-up simulation (b, d and f, respectively).

1525

1526 **Figure 5:** As Figure 4 but for concentrations at 150 m. Note that color shading does
1527 not represent the same amplitude in spatial biases as in Figures 4 and 6.

1528

1529 **Figure 6:** As Figure 4 but for concentrations at 2000 m. Note that color shading does
1530 not represent the same amplitude in spatial biases as in Figures 4 and 5.

1531

1532 **Figure 7:** Temporal-vertical evolution in root-mean squared error (RMSE) for
1533 biogeochemical tracers during the 500-year-long spin-up simulation of IPSL-CM5A-
1534 LR. RMSE is given for (a) dissolved oxygen O₂, (b) nitrate NO₃ and (c) difference
1535 between alkalinity and dissolved inorganic carbon Alk-DIC.

1536

1537 **Figure 8:** Temporal evolution of drift in root-mean squared error (RMSE) for
1538 dissolved oxygen (O₂, blue crosses), nitrate (NO₃, green crosses) and difference
1539 between alkalinity and dissolved inorganic carbon (Alk-DIC, orange crosses) during
1540 the 500-year-long spin-up simulation of IPSL-CM5A-LR. Drift in RMSE is given at
1541 surface (a,b and c), 150 m (d, e and f), and 2000 m (g, h and i) for these three
1542 biogeochemical fields. Drift in RMSE is computed from time segments of 100 years
1543 beginning every 5 years from the beginning until year 400 of the spin-up simulation
1544 for O₂, NO₃ and Alk-DIC tracers. The best-fit regressions between drifts in RMSE
1545 and spin-up duration over year 250 to 500 are indicated in solid magenta lines; their
1546 90% confidence intervals are given by thin dashed envelopes. Least square correlation
1547 coefficients are tested against a one-tailed t-test with significance level of 90% and
1548 ~15 effective degrees of freedom estimated with the formulation of Bretherton et al.,
1549 (1999) ; * indicates if a given least square correlation coefficient passes the test.

1550

1551 **Figure 9:** Scatterplot of drifts in root-mean squared error (RMSE) in O₂ concentration
1552 versus the duration of the spin-up simulation for the available CMIP5 Earth system
1553 models. Drifts in O₂ RMSE are respectively given for surface (a), 150 m (b) and 2000
1554 m (c) for oxygen concentrations. Drift in O₂ RMSE is computed from several time
1555 segments of 100 years beginning every 5 years from the beginning until the end of the

1556 piControl simulation for the available CMIP5 models. Coloured symbols indicate the
1557 mean drift in O₂ RMSE while vertical lines represent the associated 90% confidence
1558 interval. The best-fit regressions between models' mean drifts in RMSE and spin-up
1559 duration are indicated as solid green lines; their 90% confidence intervals are given by
1560 thin dashed envelopes. Fits are assumed robust if correlation coefficients are
1561 significant at 90% (i.e., $r^* > 0.34$). For comparison, drift in O₂ RMSE from our spin-up
1562 simulation with IPSL-CM5A-LR (Figure 8) are represented by magenta crosses.

1563

1564 **Figure 10:** Rankings of CMIP5 Earth system models based on standard and penalized
1565 version of the distance from oxygen observations. The standard distance metric is
1566 calculated as the ensemble-mean root-mean squared error (RMSE) for O₂
1567 concentrations at surface (a), 150 m (b) and 2000 m (c). The penalized distance metric
1568 incorporates drift-induced changes in O₂ RMSE (Δ RMSE) to O₂ RMSE at surface (d),
1569 150 m (e) and 2000 m (f). Ensemble-mean RMSE are calculated using available
1570 ensemble members of Earth system models oxygen concentrations averaged over the
1571 1986-2005 historical period relative to WOA2013 observations. Δ RMSE is
1572 determined using Equation 2 and fits derived from first century of the CMIP5
1573 piControl simulations. Solid red and magenta lines indicate the multi-model mean
1574 standard and penalized distance from O₂ observations, respectively. With the same
1575 colour pattern, dashed lines are indicative of the multi-model median for the standard
1576 and penalized distance from O₂ observations.

1577

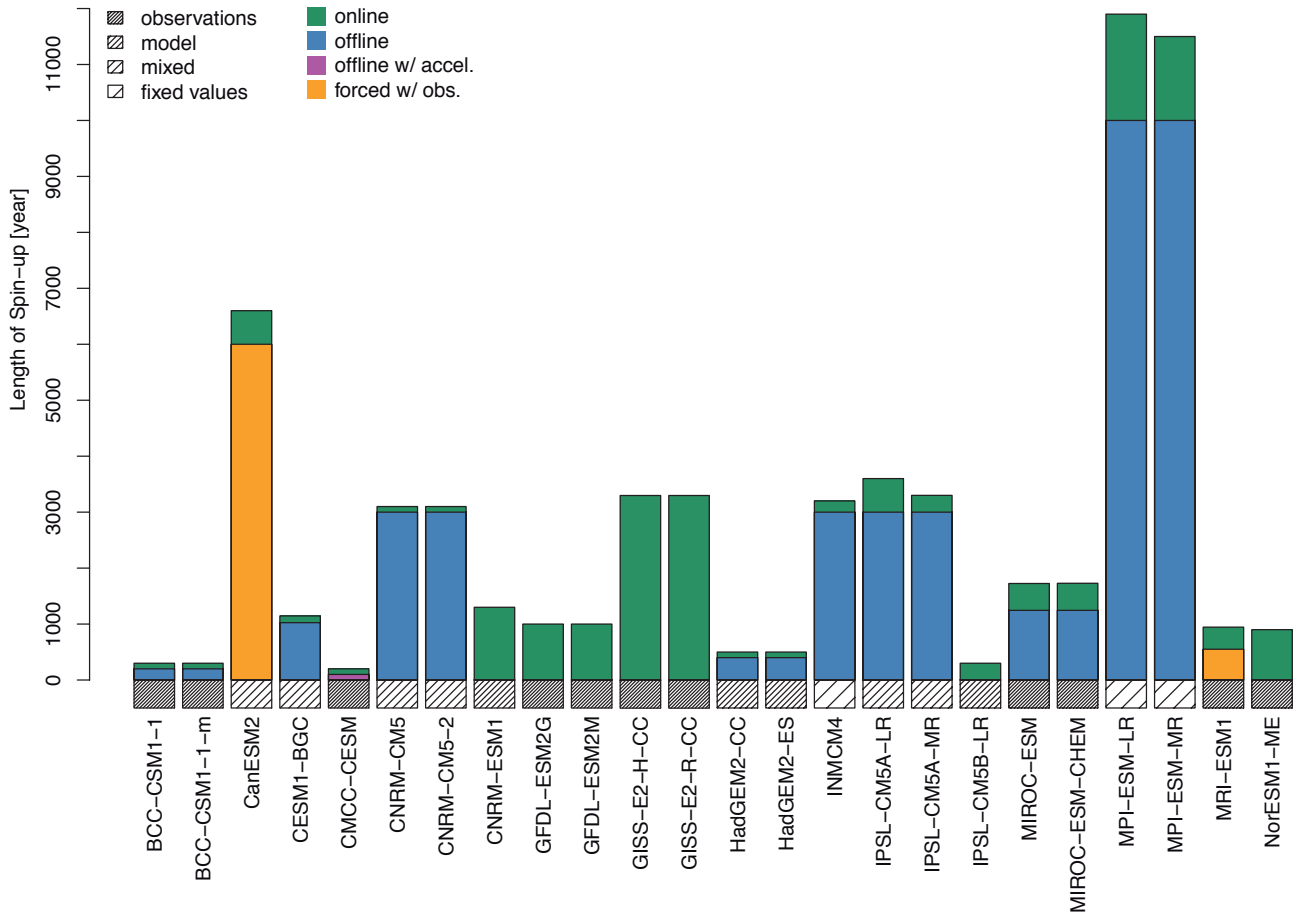


Figure 1:

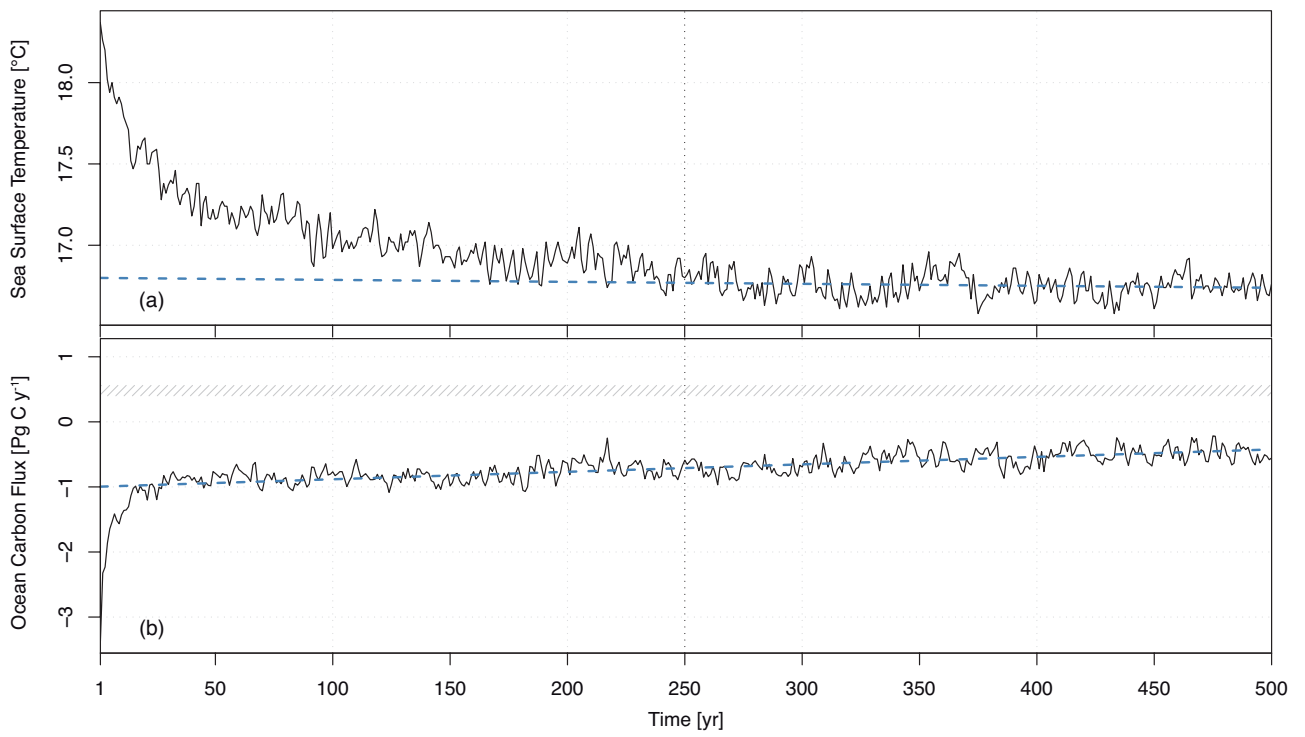


Figure 2:

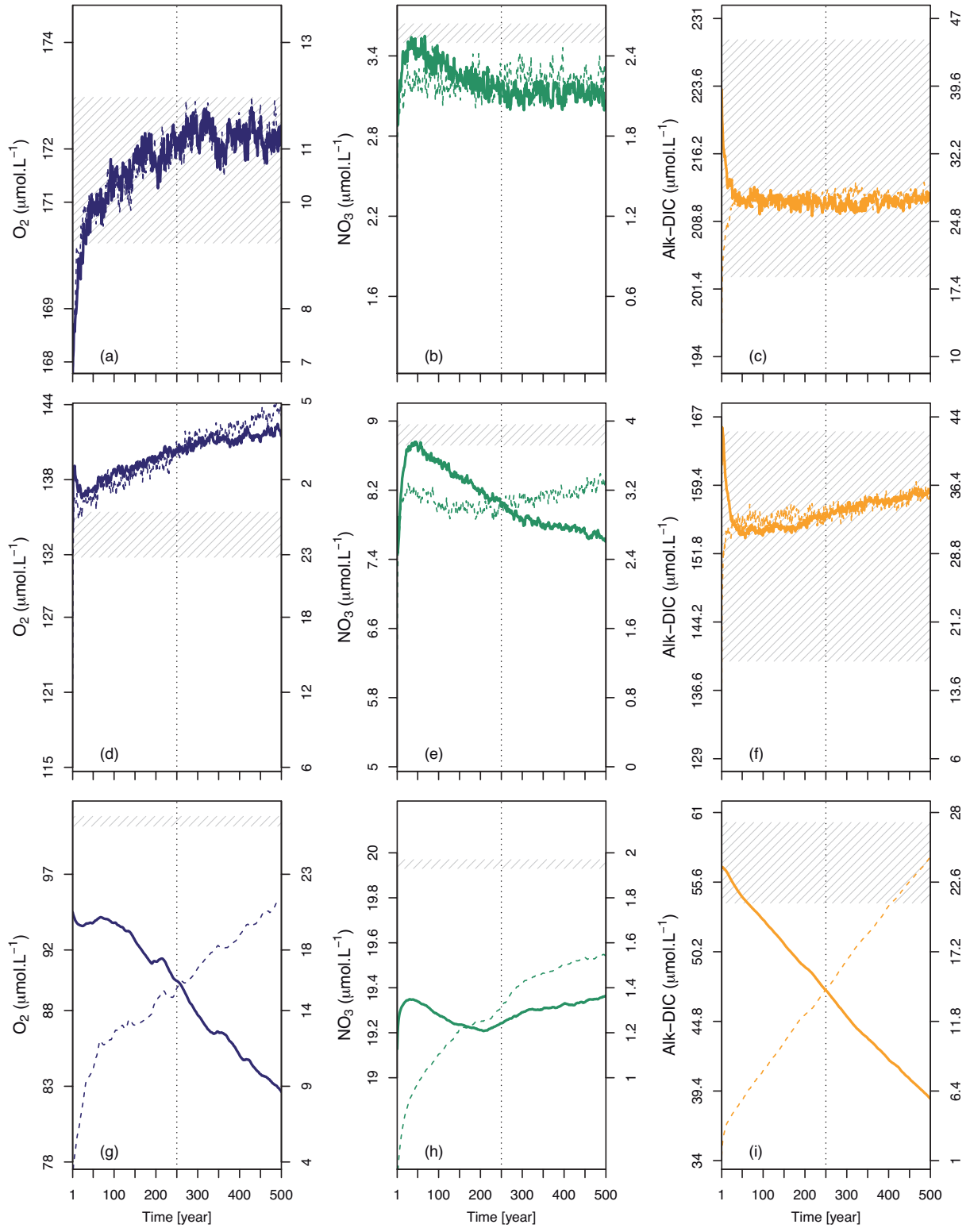


Figure 3:

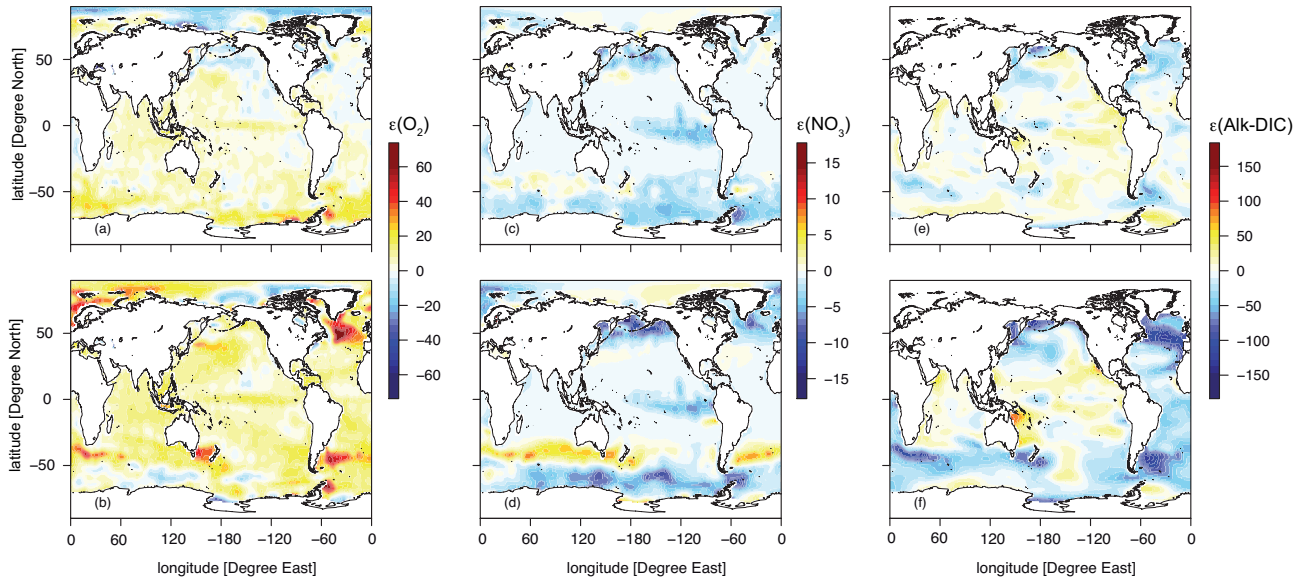


Figure 4:

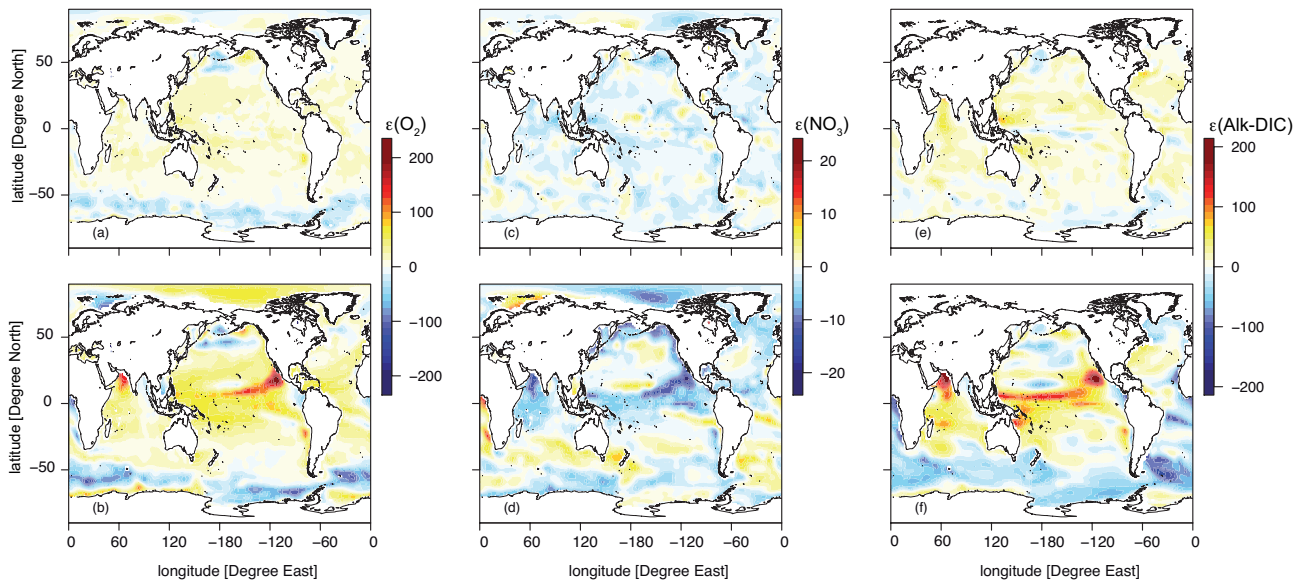


Figure 5:

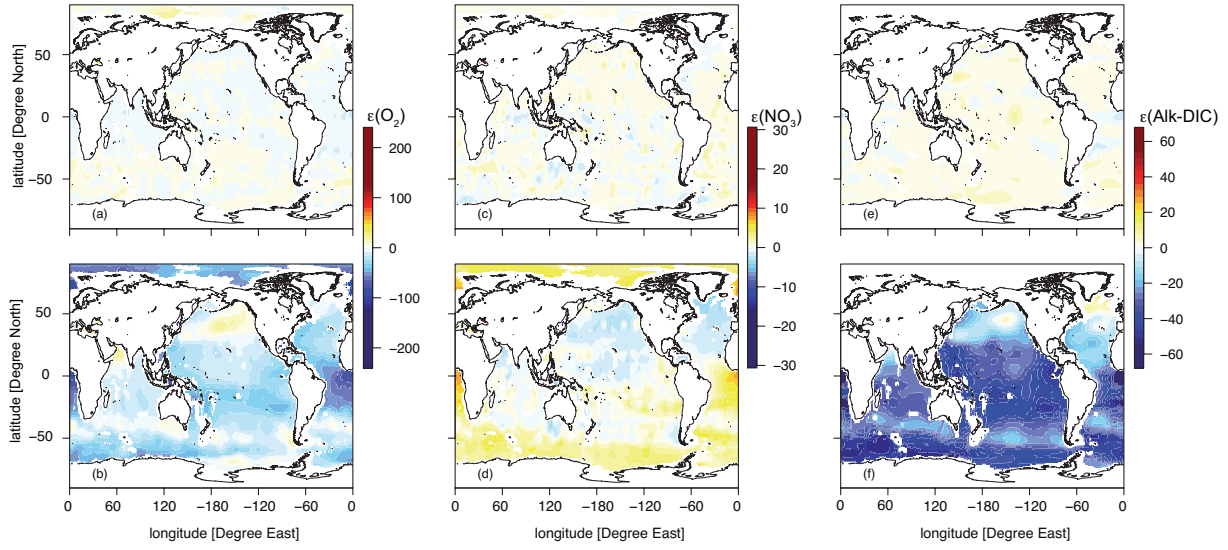


Figure 6:

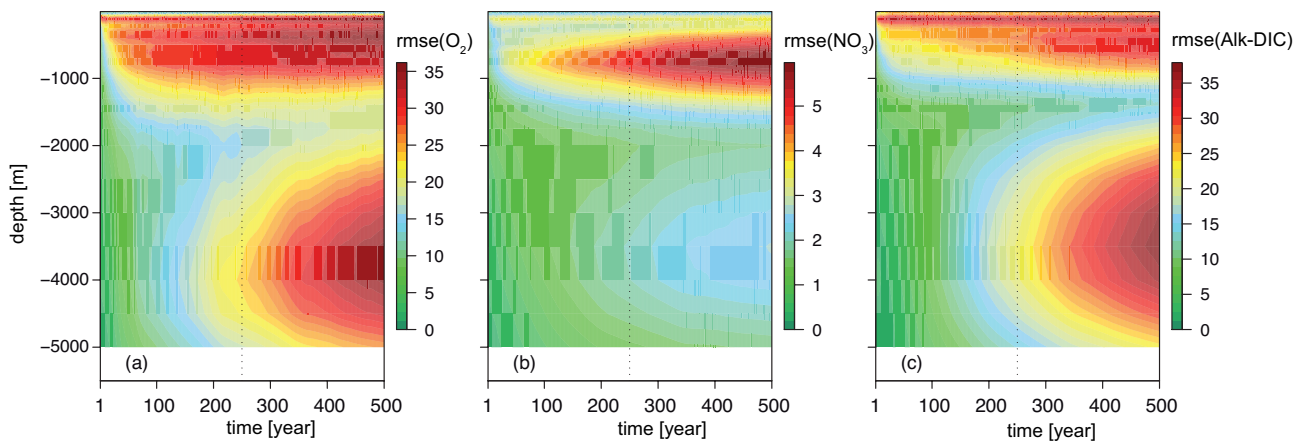


Figure 7:

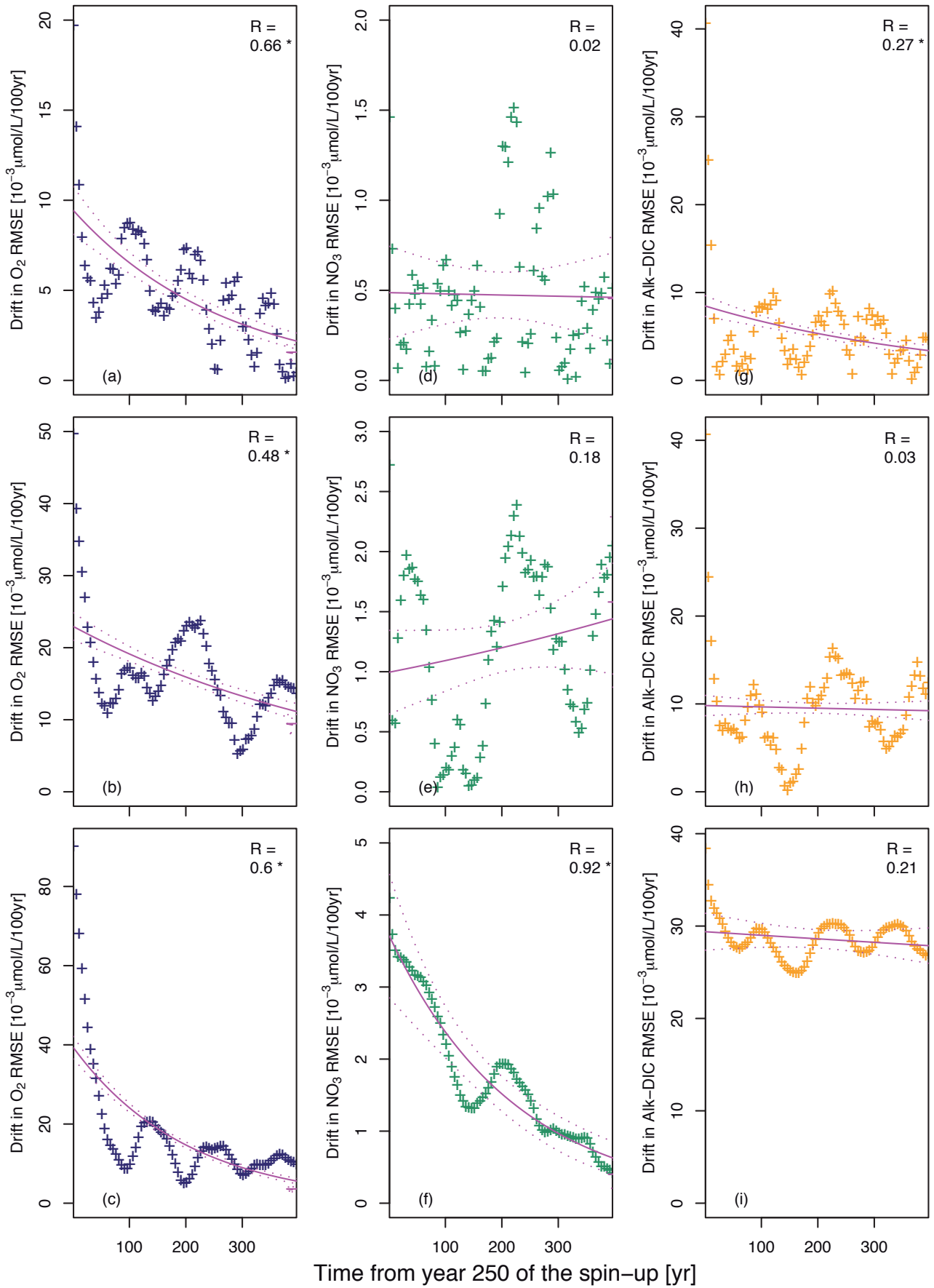


Figure 8:

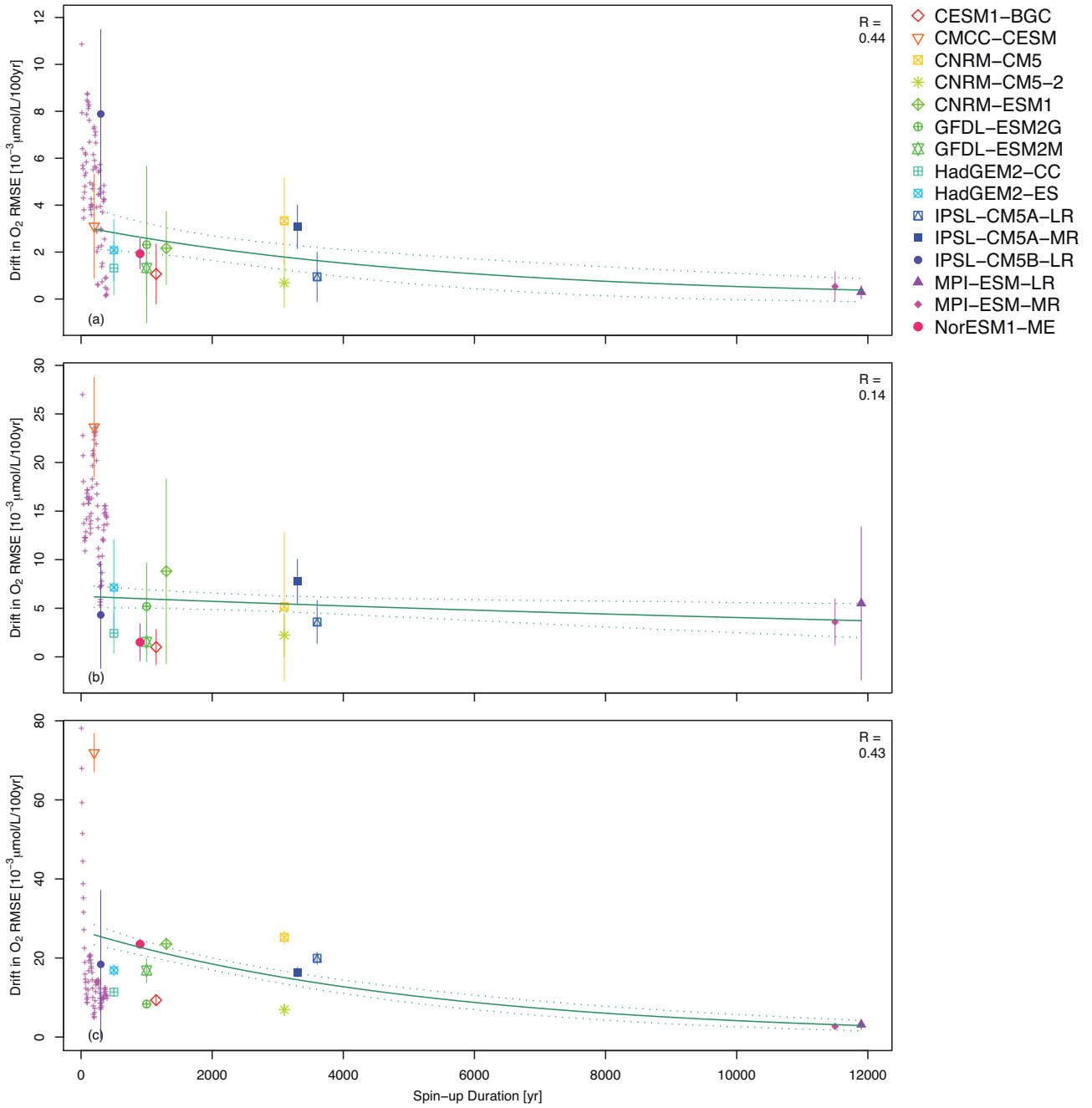


Figure 9:

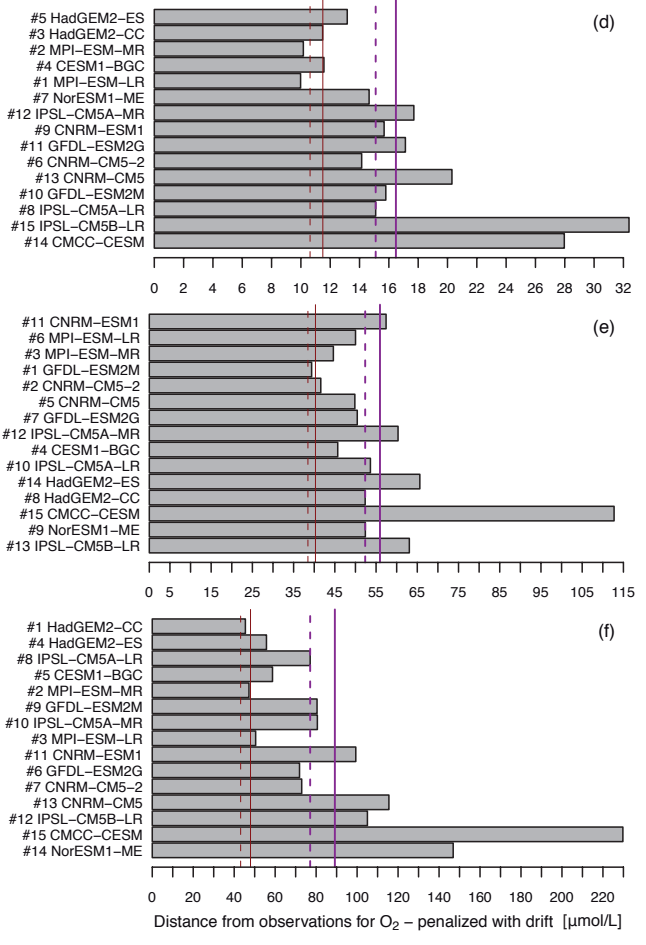
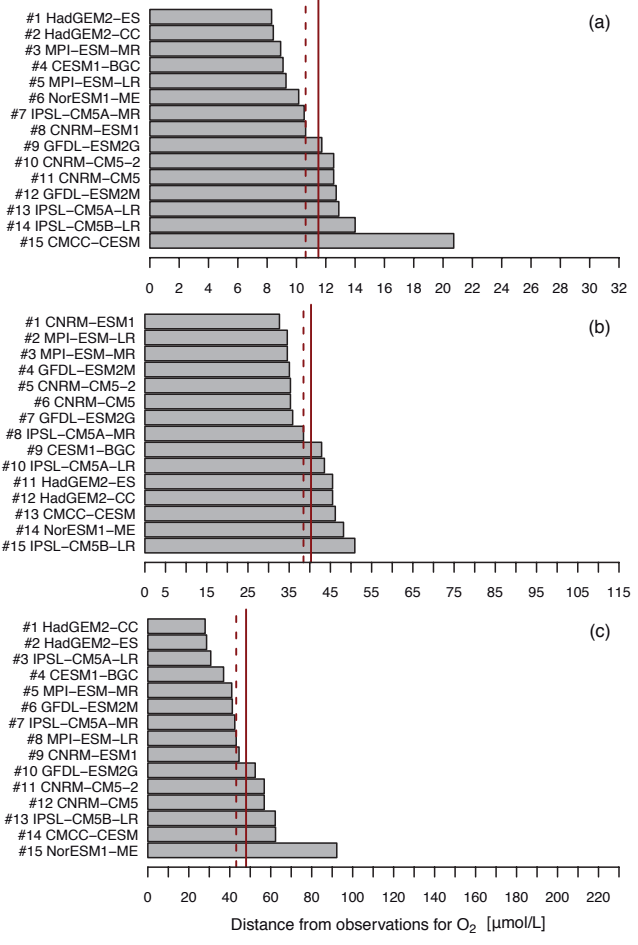


Figure 10: